Universidade Federal de Juiz de Fora

Engenharia Elétrica

Programa de Pós-Graduação em Engenharia Elétrica

Ândrei Camponogara

Measurement and Characterization of Aircraft PLC Channels

Juiz de Fora

2016

Ândrei Camponogara

Measurement and Characterization of Aircraft PLC Channels

Orientador: Moisés Vidal Ribeiro

Coorientador: Renato Machado

Juiz de Fora

2016

Ândrei Camponogara

Measurement and Characterization of Aircraft PLC Channels
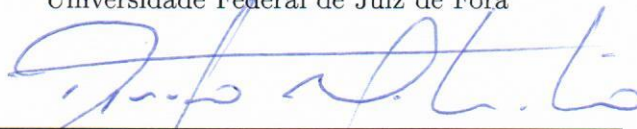
Dissertação de mestrado apresentada ao Programa de Pós-Graduação em Engenharia Elétrica da Universidade Federal de Juiz de Fora, na área de concentração em sistemas eletrônicos, como requisito parcial para obtenção do título de Mestre em Engenharia Elétrica.

Aprovada em:
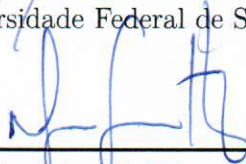
BANCA EXAMINADORA
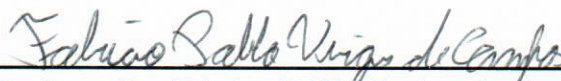
Prof. Dr. Moisés Vidal Ribeiro - Orientador
Universidade Federal de Juiz de Fora

Professor Dr. Renato Machado - Coorientador
Universidade Federal de Santa Maria

Professor Dr. Marcelo Eduardo Vieira Segatto
Universidade Federal do Espírito Santo

Professor Dr. Fabrício Pablo Virgínio de Campos
Universidade Federal de Juiz de Fora

Dedico este trabalho aos meus pais Luiz e Ivani, aos meus irmãos Gláuber e Douglas e a minha namorada Clarissa.

AGRADECIMENTOS

"Genius is one percent inspiration, ninety-nine percent perspiration."

(Thomas Alva Edison)

RESUMO

Esta dissertação tem como objetivo discutir a caracterização da rede de energia elétrica que alimenta os equipamentos de instrumentação de uma aeronave de ensaios de voo. Para a caracterização desses canais, uma campanha de medição foi realizada dentro da aeronave, de forma que dois arranjos de cabos foram adotados. Um representa a topologia em árvore, típica em aeronaves, enquanto que o segundo refere-se a uma proposta, a qual tem por objetivo compensar os problemas causados pelo modo comum através da redução do efeito de multi-percurso. No intuito de auxiliar o desenvolvimento das novas gerações de tecnologia de comunicação via rede de energia elétrica (*power line communication -* PLC) para aeronave e levando em conta o padrão aeronáutico RTCA/DO-160G, análises dos canais PLC medidos são realizadas em termos de ganho médio do canal, raiz quadrada do atraso médio de propagação, tempo de coerência, banda de coerência e capacidade do canal. Em relação ao ruído aditivo medido, análises da densidade espectral de potência e informações estatísticas são descritas. Além disso, distribuições de probabilidade são consideradas para modelá-lo e parâmetros do ruído impulsivo são discutidos. Em seguida, análises da impedância de acesso mostram importantes características dos cabos de energia elétrica utilizados para alimentar os equipamentos de instrumentação da aeronave de ensaios de voo. Por fim, comparações entre os canais PLC medidos em residências Brasileiras mostram que a tecnologia PLC disponível no mercado (desenvolvida para residências) é útil para aplicações em aeronave.

Palavras-chave: Comunicação via rede de energia elétrica. Medição. Caracterização. Aeronave. Meio de comunicação. Ruído.

ABSTRACT

This dissertation aims to discuss the characterization of the flight test aircraft power line channels related to the 28 Vdc electric power grids designed to supply energy to the instrumentation equipments. For characterizing these channels, a measurement campaign was carried out aboard an aircraft and two data communication configurations of power lines were taken into account. While one represents a typical aircraft tree-shape topology of cable bundles, the second one is a proposal aiming at compensating the common-mode problems by reducing the multipath effects. In the light of aeronautic standard RTCA/DO-160G, analyses of measured power line communication (PLC) channels in terms of average channel gain, root mean square - delay spread, coherence time, coherence bandwidth, and channel capacity gives some directions to design novel generations of PLC technology for aircraft applications. Regarding the measured additive noises, analyses based on power spectral density and evaluated statistic information are addressed. Moreover, symmetric statistical distributions are considered to model the measured additive noise. In addition, parameters of impulsive presence in the measured additive noise are discussed, and analysis of the access impedance shows some important characteristics of typical power lines used to supply energy to instrumentation equipments in a flight test aircraft. Finally, a comparison with the Brazilian in-home PLC channels shows that the PLC technology on-the-shelf (designed for in-home PLC) is also useful for aircraft applications.

Key-words: power line communication, measurement, characterization, aircraft, communication medium, noise.

LIST OF FIGURES

LIST OF TABLES

ACRONYMS

ACA average channel attenuation

ACE actuator control electronics

ACG average channel gain

AIC Akaike information criterion

BER bit error rate

BIC Bayesian information criterion

BPLC broadband PLC

cdf cumulative distribution function

CDS cockpit display system

EDC efficient determination criterion

CFR channel frequency response

CIR channel impulse response

CLS cabin lighting system

CM common-mode

CMRR differential-mode to common-mode rejection ratio

COTS commercial off-the-shelf

CSD current spectral density

DAS data acquisition system

DFT discrete Fourier transform

DM differential-mode

DS delay spread

EMC electromagnetic compatibility

FCC Fisher Custom Communication

FCE flight control electronics

FCS flight control system

HPAV HomePlug AV

HS-OFDM hermitian symmetric OFDM

HVDC high voltage direct current

ICI inter carrier interference

ISI inter symbol interference

MAC media access control

OFDM orthogonal frequency division multiplexing

OFDMA orthogonal frequency domain multiple access

OPERA open PLC European research alliance

PAPR peak to average power ratio

PC personal computer

pdf probability density function

PLC power line communication

PoD power over data

PSD power spectral density

PWM pulse width modulation

QAM quadrature amplitude modulation

QPSK quadrature phase-shift keying

RAE remote actuator electronics

RE remote electronics

RMS-DS root mean squared delay spread

ROBO robust modulation

SNR signal-to-noise ratio

TAUPE Transmissions in Aircraft on Unique Path Wires

VNA vector network analyzer

WSSUS wide-sense stationary uncorrelated scattering

CONTENTS

1 Introduction

Power line communication (PLC) systems and their applications have been widely studied by academic and business communities with the main focus on in-home (residential and commercial buildings) and outdoor electric power grids. More, recently, the PLC technology has began to be investigated in the context of transportation systems, such as ships [2], trains [3], vehicles [4], spacecraft [5], and aircraft [6].

Regarding aircrafts, we point out that approximately 15% of its weight is due to wires dedicated to condition monitoring and control, in-flight entertainment and cabin management [7]. Furthermore, there is a tendency of "more electric" aircraft since pneumatic energy sources will be replaced by electrical ones [8]. Consequently, an increase in complexity, weight and volume of electrical system is expected [9]. In this context, the use of power lines for both data communication and power delivery comes up as an interesting solution in order to alleviate the impacts on weight and aircraft assembling. In fact, the use of PLC technology has a great potential of cost-cutting in aircraft applications.

Nevertheless, as it is well known, electric power grids in vehicles as well as in other environments were not design for data communication. Actually, there were conceived to maximize energy delivery at low frequencies (DC, 60 Hz or 50 Hz, and 400 Hz,). Electric power grids are harsh media, in which the signal suffers significant attenuation with distance and frequency increase, distortion due to time varying behavior of the power line, impedance mismatching, and corruption due to high power impulsive noise presence. Also, topology diversity and unpredictable connection/disconnection of loads make such communications medium much more complicate for data communication. For those reasons, there are several contributions focusing on the measurement and the characterization of in-home and outdoor electric power grids [10–15]. However, the discussed results do not reflects the reality in aircraft harness once the geometrical characteristics and tree-shaped topologies of cable bundles and design of electric circuits are completely different from in-home and outdoor electric power grids [16].

The feasibility of PLC technology in aircraft has been proved in some works [8, 16–18]. For instance, measurements of 14 power line links on a test bench of a cabin lighting system (CLS) cell were evaluated and discussed in [16], in which magnitudes of channel frequency response (CFR) were characterized. Additionally, theoretical analyses of coherence bandwidth and delay spread (DS) [8] and measurements of access impedance of 4 points at CLS cell [19] were addressed.

The suitability of PLC technology aboard aircraft was verified by injecting a PLC signal into two power lines - differential-mode (DM), rather than between a single power

line and the ground - common-mode (CM)[1]. The analysis related to both CM and DM are relevant because the electromagnetic compatibility (EMC) constraints imposed by the aeronautic standard RTCA/DO-160G [20], in which the conducted/radiated emissions are given in terms of CM current.

After a careful review of literature, we could note that all reported measurement campaigns refer to experiment conducted at laboratory facilities, except [6]. Also, there is a lack of comprehensive characterization of aircraft PLC channel, since information such as coherence time was not found in the literature. Therefore, detailed measurement campaigns are needed for better characterizing these media in order to support the development of new generations of PLC technology for aircraft. Currently, there are few products on-the-shelf for aircraft PLC systems and all of them are based on chipset developed for in-home PLC systems.

1.1 Objectives

Based on the aforementioned problems and motivations for the characterization of aircraft PLC channels, the main objectives of this dissertation are the following:

- To perform a measurement campaign at a flight test executive aircraft Legacy 450, specifically on the harness that deliveries energy for instrumentation equipments of flight tests, so that two configuration of power lines (CF #1 and CF #2) are used to connect the measurement devices to the aircraft electric circuits covering the frequency band $1.7 - 100$ MHz. While CF #1 represents a typical aircraft thee-shaped harness configuration, CF #2 describes a new proposal that is more suitable for PLC systems.

- To statistically characterize the frequency response magnitude, ACA, coherence bandwidth, RMS-DS, coherence time, channel capacity, additive noise, and access impedance.

- To analyze and compare the CFR estimates and the results presented in [13] to verify if the in-home PLC technology can be used for aircraft PLC applications.

1.2 Dissertation outline

The rest of the document is organized as follows:

- Chapter 2 outlines a comprehensive review about PLC technology in aircraft.

---

[1] The CM characterizes the wiring configuration usually used in aircraft, where its chassis is used as ground.

- Chapter 3 presents the measurement configurations CF #1 and CF #2, such that the last one represents the proposal of this dissertation, and setups used in the measurement campaign aboard the aircraft. Also, performance metrics considered to assess the collected data set are addressed.

- Chapter 4 describes the numerical results of the data assessment and compares the CFR results with the Brazilian in-home ones [13].

- Chapter 5 addresses the concluding remarks of this dissertation.

2 State of Art: Aircraft PLC

The search for solutions to reduce wiring complexity in aircraft systems has been pushed a growing interest in the use of PLC technology [6, 21–23]. Consequentially, on September 1st, 2008, the European Transmissions in Aircraft on Unique Path Wires (TAUPE) project was initiated through a partnership between business and academic communities [9, 16–19, 24–26]. The main goal of this project was to investigate the feasibility of PLC and power over data (PoD) technologies aboard a commercial aircraft as a solution to the increase of number cables and system complexity. The 28 Vdc and 115 Vac (single-phase) power lines of A380 Airbus aircraft was adopted for the investigation, so that two reference scenarios for PLC application - CLS and cockpit display system (CDS) - were considered. Since then, many works about PLC aboard aircraft has been published. In order to highlight the advances in this field, this chapter presents comprehensive review about aircraft PLC in chronological order.

In this context, it is worth to point out that [21] is the first paper published about the use of PLC aboard aircraft dated 2002. In this paper, Godo proposed a flight control system (FCS) based on Boeing's large airplane, in which the Boeing 777's actuator control electronics (ACE) was replaced by remote actuator electronics (RAE). In order to solve the increased aircraft weight due to the flight control wiring, this work considered a PLC system as a solution. The data communication was made by replacing the aeronautic radio INC (ARINC) 429^1 communication data protocol by MIL-STD-1553^2 running at the same speed. The PLC signal was magnetically coupled (inductive coupling) on two 28 Vdc power lines by using DM signal propagation. Considering a large aircraft (> 400 passengers), the PLC-based FCS resulted on a wiring weight reduction of approximately 900 lb ($\approx$ 408 kg). However, the costs associated with wiring reduction were negligible. On the other hand, for a smaller aircraft, [21] reported that the gains added by PLC-based FCS is not valuable in relation to weight and cost savings.

In 2006, [6] reported measurements of CFR on 28 Vdc power grid of a military aircraft. A frequency band $10 - 100$ MHz and two links for the measurement were considered: (i) link #1 was from the left wing to the right wing, and (ii) link #2 was from the left wing to under the cockpit on the right side. Besides, the paper portrayed a discussion about the design of PLC-based data communication hardware and processing time constraints for PLC system in aircraft.

In [22], authors investigated the use of broadband PLC (BPLC) in frequency band $1 - 30$ MHz aboard C-27J transport aircraft. The PLC channel was modeled considering

---

^{1} ARINC 429 is a technical standard predominant in avionic's field that defines the physical and electrical interfaces for avionic data bus [27].

^{2} MIL-STD-1553 is a military standard that defines physical, mechanical, and electrical interfaces design for avionic data bus [28].

a real installation setup of an aircraft 28 Vdc power grid, which was based on DM propagation. This setup included a load, bulkhead connectors, and transmitter and receiver devices. The results showed that multi-carrier modulation and DM signal propagation reduced the intensity of radiated emission. Also, authors noted that the use of better models for connectors and transmission lines (RF models) by taking into account the parasitic parameters of connectors can offer a more realistic channel model.

Feasibility of PLC technology aboard aircraft was evaluated in the context of FCS with RAE in [23]. In this work, PLC channel analyses were carried out among flight control electronics (FCE) and remote electronics (RE). The proposed PLC system on 28 Vdc power grid was based on quadrature phase-shift keying (QPSK) modulation with orthogonal frequency domain multiple access (OFDMA) scheme. The results showed that the OFDMA scheme could achieved a bit rate of 2 Mbps per RE in a network encompassing up to 5 REs for a frequency band $2-50$ MHz. Also, the critical analysis of the OFDMA-based PLC system resulted in a potential 17.45 kg weight savings when used as backup communication scheme. Besides, the work concluded that PLC system cannot be used as primary communication system because of the presence of circuit breakers. The data link must be maintained between FCE and RE if the breaker is opened, so that the RE continues to be monitored. Even if the FCE could start the backup communication system, this is not a situation suitable for critical systems in avionic field.

Regarding the TAUPE project, the first paper came up in 2009. Considering the CLS as a scenario for PLC system in aircraft, Junqua et al. [24] introduced a propagation model for a frequency band $0.1-50$ MHz (narrowband and broadband). The results showed maximum attenuation and delay spread around 36 dB and 4 μs, respectively.

In 2010, [25] discussed the feasibility of PLC system based on open PLC European research alliance (OPERA) specifications for the aircraft's CLS environment. PLC channel characteristics were obtained from theoretical propagation model by assuming two signal propagation modes: CM and DM (untwisted lines). A frequency band from 100 kHz up to 50 MHz was considered. Four power line links with distances of 11.94 m, 17.97 m, 40.13 m, and 42.75 m were analyzed. The worst power line link (40.13 m) for CM showed maximum attenuation around 60 dB and minimum attenuation around 17.5 dB. For DM propagation, the worst power line link (42.75 m) showed maximum and minimum attenuation around 64 and 18 dB, respectively. Preliminary statistical analysis for CM and DM propagations showed that the channel behaviors were not strongly dependent of the distance between bundle and ground. Also, they were not strongly different for CM and DM propagations in terms of statistical characteristics. Moreover, maximum and mean values of coherence bandwidth found were 1.6 MHz and 600 kHz, respectively, while the maximum delay spread was 800 ns. Performance results in terms of bit error rate (BER) were presented only for CM propagation. They suggested that a BER of 10^{-4}

may not be reached in the worst link (40.13 m) due to the constraint on transmission power imposed by aeronautic standard RTCA/DO-160G [20]. Hence, the paper indicated that the DM propagation is an option to improve the PLC system performance.

A simulation tool of point-to-point PLC system for aircraft 115 Vac (400 Hz) power grid was introduced in [7]. This simulation tool encompassed a model of PLC channel based on transmission line theory, a model of 115 Vac (400 Hz) power supply in compliance with different international aeronautic standards for power supply systems, and an uncoded orthogonal frequency division multiplexing (OFDM) scheme based on quadrature amplitude modulation (QAM). Besides, the authors presented the first state of art about PLC systems focused on aircraft application.

In [29], Kilani et al. presented a noise measured campaign carried out in laboratory on three-phase shielded power lines of 10 m length between an inverter and a motor. The motor was fed by a pulse width modulation (PWM) frequency inverter with switching frequency of 15 kHz. Measurements were performed with a Fisher Custom Communication (FCC) probe current (F-65 model). In the time domain, the noise was collected through two GageScope waveform digitizer boards installed in a computer with sampling frequency of 200 MHz. Measurements in frequency domain were performed with vector network analyzer (VNA) considering frequency band from 500 kHz up to 50 MHz on 1601 points. Also, the performance of PLC channel based on the HomePlug AV (HPAV) and on the OPERA-Type I specifications was presented. The results showed a mean degradation of BER due to PWM frequency inverter. Also, a BER of 10^{-5} is reached with a signal-to-noise ratio (SNR) of 6 and 11 dB for HPAV and OPERA specifications, respectively, so that the HPVA obtained a gain of 5 dB in terms of SNR in relation to OPERA.

In order to continue the studies described in [24] and [25], [17] presented numerical assessment of aircraft PLC channel in context of CLS environment. This work analyzed the characteristics of PLC channel for the frequency band $1 - 50$ MHz through a theory of multi-conductor lines-based model. CM and DM (untwisted lines) propagations were adopted. Results from theoretical model allowed the extraction of relevant parameters for analysis of power line link to design and to built a test bench. From this test bench, a numerical model of the CLS was developed and validated for the frequency band $1 - 30$ MHz by comparing simulation and measurement results. Exhaustive numerical simulations of data transmission were performed in order to obtain a final representative PLC channel model. Also, EMC aspects and crosstalk inside the harness[3] were discussed.

Regarding the use of PLC technology aboard aircraft, [18] verified the advantages of DM propagation in relation to CM one. Results showed the following advantages when

---

[3]   The harness term represents the total electric power network of a specific system in an aircraft.

DM propagation is adopted: (i) decrease of crosstalk effect inside the bundle; (ii) increase of power spectral density (PSD) of the received signal (less signal attenuation); and (iii) reduction of conducted and radiated emissions levels from the power line. Measurements on test bench for the frequency band $1-50$ MHz showed a gain up to 50 dB in terms of SNR for DM propagation in relation to CM one. Finally, EMC measurements indicated even with a transmission signal with PSD up to -50 dBm/Hz, compliance with aeronautic standards RTCA-DO160G [20] could be reached when DM is considered. At the end, this paper presented a system to detect cable fault (broken wire or increased contact resistance) considering DM propagation.

In [26], adopting CLS as scenario for data communication, authors analyzed the performance of aircraft PLC system for CM and DM propagations, in terms of BER, for 14 power line links. Results indicated that CM propagation was not feasible for a bit rate higher than 15 Mbps due to upper limit over current flowing (20 dBμA/kHz) imposed by aeronautic standard RCTA/DO-160G [20]. On the other hand, DM propagation, in compliance with the aeronautic standard, allowed data communication through all 14 power line links by reaching a data rate of 30 Mbps with BER less than 10^{-3} for a bandwidth of 30 MHz (OPERA-Type I specifications).

Dominiak et al. [30] performed measurements of conducted and radiated emissions related to the PLC signal transmission through two power lines (DM propagation). The measurement setup was built in compliance with the aeronautic standard RTCA/DO-160G [20] and tests were performed on a shielded semi anechoic room. Results showed that measured levels of conducted emissions were in compliance with the limitation imposed by aeronautic standard RTCA/DO-160G. However, regarding radiated emissions, anomalies were found in measurements made with a rod antenna in the frequencies below 25 MHz, apparently because of OFDM signal nature (high peak to average power ratio - PAPR).

Results discussed in [17,24,25] were republished in [31], besides some new analyses in relation to EMC aspects and throughput of the power line link. Measurements related to EMC were carried out injecting a disturbing signal on a neighboring line of two twisted power lines envisaged to PLC system, so that the disturbing signal current does not exceed 20 dBμA/kHz in frequency band considered ($1.8-30$ MHz). Results showed an average coupling loss around 10 dB and that the DM to CM rejection ratio (CMRR)[4] remains greater than 10 dB. In relation to the performance of power line link, extensive numerical simulations were carried out, so that HPAV specifications were considered for both CM and DM propagations. In this sense, a BER of 10^{-3} was fixed and the upper limit of current flowing in CM was 20 dBμA/kHz. Therefore, the throughput found in a CM propagation only could reach low bit rate for a short distance of power line link. However,

---

[4]   The CM rejection ratio is given by $CMRR = I_{CM}/I_{DM}$, where I_{CM} is the CM current and I_{DM} is the DM current.

for DM propagation, the throughput varied between 12 Mbps and 62 Mbps, according to the type of link.

In [9], authors presented results of functional and performance tests considering commercial off-the-shelf (COTS) PLC modems base on OPERA specifications. Also, it is described an overview about PLC technology, commercial BPLC standards, and aircraft PLC channel characteristics. Analyses considering frequency band $2 - 30$ MHz showed that the aircraft PLC channel could provide a throughput of 100 Mbps with low latency times (< 5 ms). However, some deficiencies were found regarding network setup time[5], efficient support of multi-cast/broadcast data delivery and media access control (MAC) scheduling algorithm.

Preliminary results from [17, 24–26, 31] were extended in [8]. This work presented analyses of aircraft PLC channel comparing CM and DM propagations in terms of throughput for 14 distinct power line links. From a theoretical model based on theory of multi-conductor transmission line, the magnitude of the aircraft PLC channel response was analyzed. Essentially, [8] showed that the loads of neighboring wires have strong influence on the magnitude of the PLC channel frequency response for a few frequency bands when CM is adopted. Also, comparing CM and DM propagations, the results indicated that their behaviors were quite similar and the loads configurations of the neighboring wires did not presented strong impact on these results. The minimum coherence bandwidth found for correlation level of 0.9 was wider than 0.6 MHz and 0.9 MHz for CM and DM propagations, respectively. For PLC channels with mean values of magnitude response around -20 dB, the maximum delay and the maximum delay spread found were 0.7 μs and 0.1 μs, respectively, considering both propagation modes. Finally, the throughput of a PLC system was analyzed through a simulation tool based on HPAV. It was considered 14 power line links and a fixed BER of 10^{-3}. So, DM propagation obtained a throughput between 62 Mbps (closest receiver, with distance of 11.6 m) and 18 Mbps (farthest receiver, with distance of 42.5 m), whereas CM propagation could offer few bits per second.

The use of three-phase power lines between a motor and a PWM inverter, which is supposed to be installed in an aircraft, as data communication medium was discussed in [29] and continued in [32]. In [32], the impulsive noise was characterized considering rotation speed of the motor such that a model for it was proposed. Also, performance of PLC modem considering the robust modulation (ROBO) configuration of HPAV [33] was analyzed in terms of BER by considering the influence of the motor speed. The result showed that the speed rotation of motor had a small impact on BER when the PLC system is based on HPAV.

---

[5] Time required to power on and connect PLC equipments to PLC network and to deliver the application data traffic

In order to mitigate PAPR, narrowband interferences, and impulsive noise, [34] proposed a non-continuous interferometry OFDM (NCI-OFDM) scheme for PLC aboard aircraft. NCI-OFDM scheme showed a gain when compared with non-continuous OFDM (NC-OFDM) in terms of BER and PAPR reduction. However, this work described that the author's focus was on PLC aboard aircraft, but the models of PLC channel considered was developed for in-home and outdoor PLC channels. This choice could be a problem because geometrical characteristics and tree-shaped topology of aircraft power lines are totally different [35].

Aiming to optimize some OFDM parameters considering a high voltage direct current (HVDC) power line between control unit and power inverter (aircraft FCS) as a data communication medium, [36] reported a measurement campaign. This report was based on the adoption of the following configurations: (i) point-to-point architecture with capacitive coupler, (ii) point-to-point architecture with inductive coupler, and (iii) point-to-multipoint architecture with inductive coupler. Measurements were carried out with VNA in a frequency band $1 - 100$ MHz with a 5 kHz resolution. With a probability of 0.1 the values of magnitude frequency response were equal to or less than -40 dB for inductive coupler in both configurations and -30 dB for capacitive coupler. Besides, for a probability of 0.5 the values of magnitude frequency response were equal to or less than -20 dB for point-to-point with inductive coupler and around -22.5 dB for other configurations. Results of coherence bandwidth apparently did not have strong dependency on respect to coupling type (capacitive or inductive), varying between 0.7 MHz and 1 MHz, whereas the delay spread varied from 78 ns up to 104 ns. From measurements results, parameters of an OFDM scheme were optimized, so that the subcarriers spacing was suggested to be equal to 70 kHz, which is around three times the value provided by HPAV specifications (24.414 kHz). Also, from the calculus of inter symbol interference (ISI) and inter carrier interference (ICI) the length of cycled prefix (L_{cp}) was reduced to 15 samples, which corresponds to 500 ns (by assuming a sampling frequency equal to 60 MHz). Hence, the OFDM symbol duration, based on the analysis of measured data set, was 14.78 μs instead of 46.52 μs (HPAV).

In [37], authors extended the studies from [29] and [32] in order to introduce a software tool to simulate PLC channels between a motor and a PWM inverter. Measurements of impulsive noise were carried out aiming to characterize it. Also, a signal processing technique was proposed to mitigate the impulsive noise presence. Measurements on test bench showed that, for a main frequency of 50 Hz, the average duration of pulses was around 2 μs, whereas the time between two successive pulses was less than 40 μs. Assessments of PLC system based on the HPAV [33] and the GreenPhy [38] specifications were carried out in order to analyze its performance. Results showed that, combining turbo codes and the technique to mitigate the impulsive noise with fixed data rate of 20 and 5 Mbps, a BER of 10^{-3} with a transmission signal PSD of -65 dBm/Hz could be reached

in the frequency band $1.8 - 30$ MHz.

The discussion presented in [36] was extended in [39]. Taking into account the aeronautic standard RTCA/DO-160 [20], Larhzaoui et al. [39] carried out a study of OFDM-based PLC system between the control unit and electrically powered actuators for FCS. They analyzed two frequency bands: $1 - 37$ MHz and $1 - 73$ MHz, by focusing on DM propagation. The results showed that the point-to-point architecture with inductive couplers achieved the best results in terms of CMRR and bit rate. Also, it stated that the increase of CMRR leads to a higher SNR and, as a consequence, the constellation size can increase. For instance, QPSK is adopted for CMRR = 15 dB while 16-QAM for CMRR = 25 dB.

As described in [8], PLC system may not be useful for high data rate application aboard aircraft through CM propagation because the regulation imposes severe constraint over current spectral density (CSD). Therefore, [16] analyzed just DM propagation. Measurements of aircraft PLC channel on a test bench were performed considering 14 power line links in order to obtain the CMRR and near-end crosstalk at the receiving points. The analysis of the CMRR showed values equal to or less than -25 dB for a probability of 0.8, which allows to use a CSD of 45 dBμA/kHz (equivalent to a PSD of -58 dBm/Hz on an impedance of 50 Ω) for the transmitting signal, instead of 20 dBμA/kHz for CM propagation. Besides that, the near-end crosstalk found was equal to or less than -28 dB for a probability of 0.8. Since the current of an additive noise of a disturbing wire can not exceed 20 dBμA/kHz, the DM current noise was around -8 dBμA/kHz. A software tool based on HPAV specifications was used to predict the performances of a PLC system in terms of BER and bit rate considering the data transmission between two PLC modems. The input data of this software was the CMRR and near-end crosstalk for a probability equal to or less than 0.8 and the CFR estimate obtain through multiconductor transmission line theory. Throughput results computed by the simulation tool for the frequency band $1.8 - 30$ MHz were equal to or less than 91 Mbps with a maximum BER of 2×10^{-4}.

An overview about theoretical and experimental approaches for the use of PLC system aboard aircraft was described in [19]. Besides, the input impedance was measured at four points of the aircraft harness through a VNA. Measurements showed that values of absolute impedance can vary approximately between 16 and 240 Ω. For a probability equal to 0.5, the absolute value of impedance found was equal to or less than 61 Ω. Moreover, characterization and modeling of PLC channels in transportation systems, such as vehicles, spacecraft, and aircraft were outlined in [35], so that their topology and functional aspects were described.

Envisaging application aboard aircraft, [40] proposed a hardware-based design and verification process for the physical layer of PLC system. The hardware-based design was made up for two different levels: conceptual design model and detailed design model.

Conceptual design model provided a high level abstraction of each component of PLC physical layer through combination of Mathworks Simulink blocks and Matlab code [41]. The detail design model encompassed the hardware requirements and the conceptual design model through a graphical representation of hardware design developed in Xilink System Generator (SysGen) [42]. Also, simulation of the executable models was used in order to provide a initial verification of the conceptual design model against the hardware requirements and to check if the conceptual design model and detailed design model has the same behavior.

After this literature review, we can note that the majority of the works related to PLC technology applied to aircraft focused on the frequency band between 1.8 and 30 MHz and only few contributions extended this frequency band. Besides, civil, military, and transportation aircrafts were investigated mainly focusing on FCS and CLS for PLC applications. Also, the works stated that due to EMC constraints imposed by aeronautic standard RCTA/DO-160G [20], the use of PLC aboard aircraft is feasible just for DM propagation. However, excepting [6], all CFR estimates and additive noise were based on measured data set obtained at laboratory facilities that emulate the electric circuits of an aircraft. Relevant informations about aircraft PLC channels behavior were not completely reported in literature, as coherence time of aircraft PLC channels. Additionally, a detailed analysis of access impedance is needed, once this information is superficially discussed. Finally, any work addressed PLC systems for instrumentation equipments boarded in flight test aircraft. Also, the quantity of works related to PLC system applied aboard aircraft is small. The main reason behind that is the reduced number of aircraft manufactures and the extremely difficult and cost to access an aircraft for carrying out analysis.

2.1 Summary

This chapter presented a review about the use of PLC technology in aircraft, by emphasizing the most relevant issues.

3 Aircraft PLC Channel

As it is well known, electric power grids were not conceived for data communication purposes. They are a harsh media, in which the signal suffers significant attenuation with distance and frequency increase, multipath phenomenon related to impedance mismatching, and the presence of high power impulsive noise associated with load's dynamics (steady state as well as connection and disconnection). Therefore, there are several contributions focusing on the measurement and characterization of in-home and outdoor electric power grids by considering both narrowband ($0 - 500$ kHz) and broadband ($1.7 - 100$ MHz) channels [10–15]. However, the discussed results do not reflect the reality in aircraft harness once the geometrical characteristics and tree-shaped topologies of cable bundles and design of electric circuits are completely different in comparison with in-home and outdoor electric power grids [16]. Thus, in order to increase the knowledge and understanding of usefulness of PLC technology in aircraft, this chapter describes a measurement campaign, which was performed in a flight test aircraft, specifically, in the 28 Vdc electric power grid that delivery electric energy to instrumentation equipments. In addition, it briefly and concisely describes the main parameters used to quantify the behavior of such power lines. The parameters are average channel gain (ACG), RMS-DS, coherence time, coherence bandwidth, and channel capacity. Finally, this chapter briefly describe the algorithm used in the PSD calculus of the additive noise and the information criteria considered to evaluate the suitability of statistical distributions used to fit the additive noise data set.

This chapter is organized as follows: Section 3.1 shows the measurement configurations and setups. Section 3.2 describes the measurement campaign. Section 3.3 outlines the parameters used to characterize the measured PLC channels. Section 3.4 defines the metrics considered to quantify the suitability of statistical distributions to model the measured additive noise.

3.1 Measurement Configurations and Setups

In order to obtain CFR, additive noise, and access impedance data sets from the 28 Vdc electric power grid of instrumentation equipments in a flight test aircraft, we adopted two measurement configurations of power lines, named CF #1 and CF #2. The main difference between both configurations is that PLC modems are connected to the electric power grid with distinct configurations.

Figure 1 depicts a PLC system where each data acquisition system (DAS) is connected to a distinct pair of PLC modems. The PLC modems A, C, and E receive the data via Ethernet interface from their own DASs and inject the PLC signals carrying their respective data into the power line. Then, the PLC modems B, D, and F collect
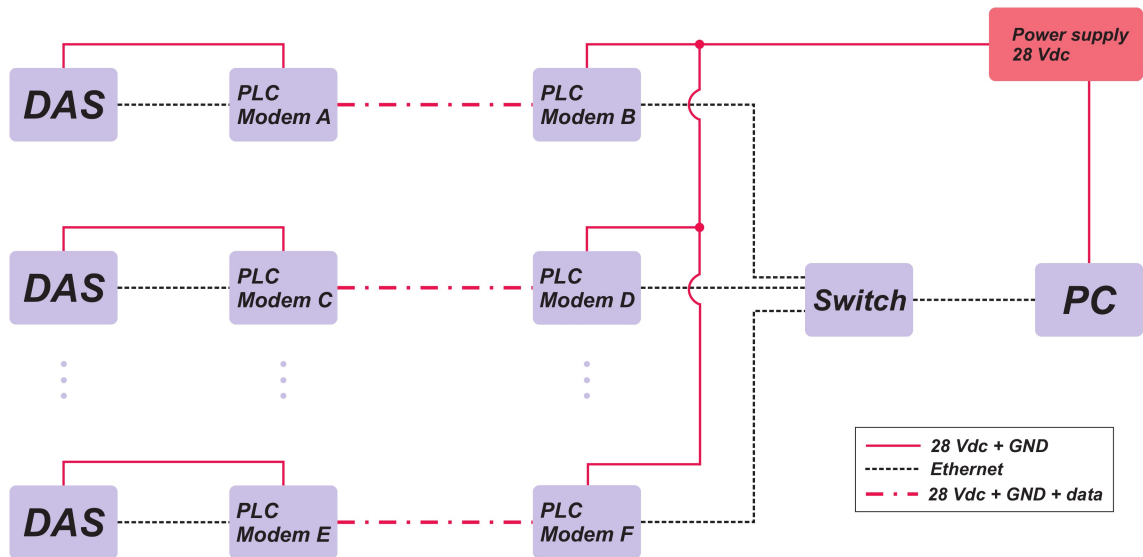
Figure 1: Illustration of a PLC system based on CF #1.
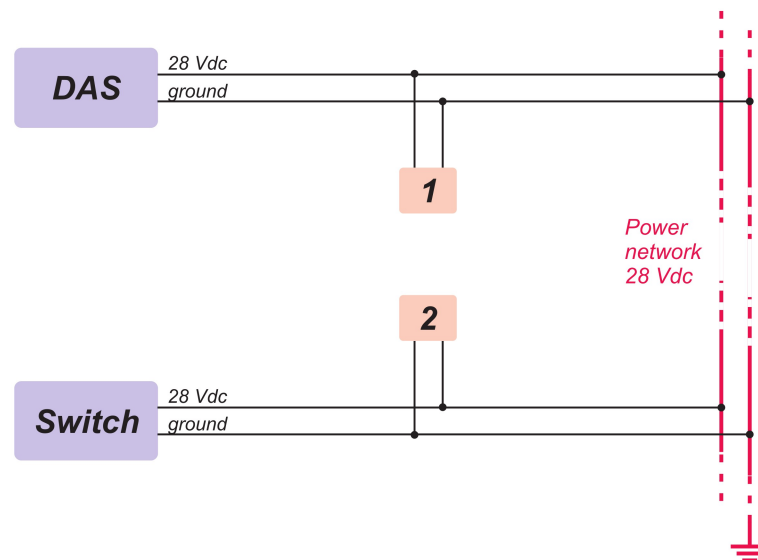
Figure 2: Illustration of the measurement configuration CF #1.

the distorted PLC signals and delivery the received data to a personal computer (PC) through a switch. Hence, in order to obtain CFR, additive noise, and access impedance estimates of such PLC channel, the CF #1 was taken into account. Figure 2 shows the block diagram for CF #1, such that the blocks #1 and #2 are the PLC modems, in which two loads, DAS and switch, are connected to a 28 Vdc electric power grid through different wire harnesses ($\approx$ 9m of length), so that there is no clear physical connection between these two PLC modems. This configuration represents the current tree-shaped topology of the aircraft harness.

Figure 3 shows a PLC system, in which the PLC modems and the flight test equipments (DAS and switch) are physically interconnected, since there is one direct and physical defined path between both of them. As illustrated in Figure 3, the DAS devices
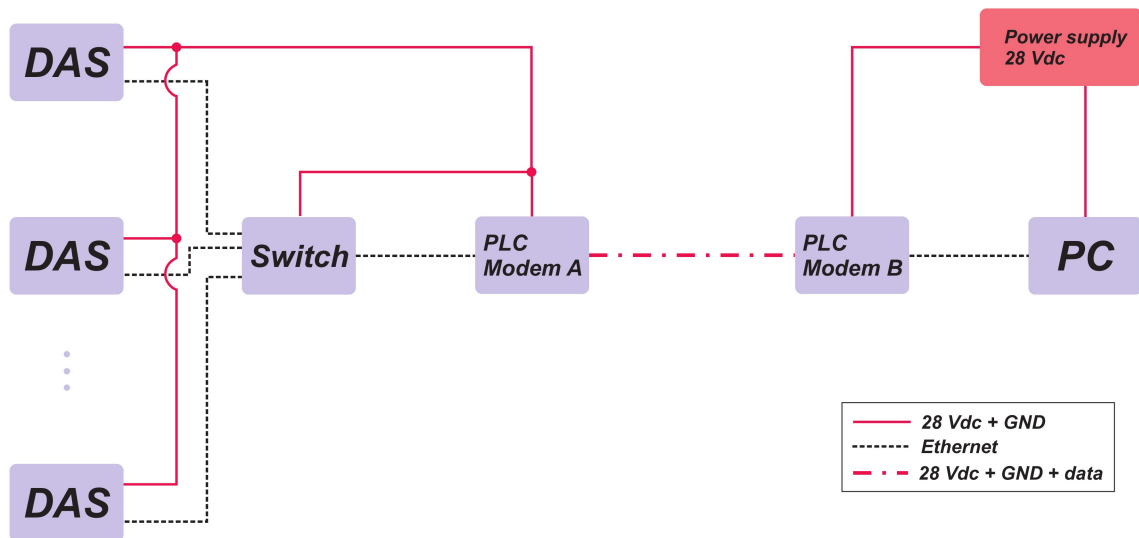
Figure 3: Illustration of a PLC system based on configuration CF #2.
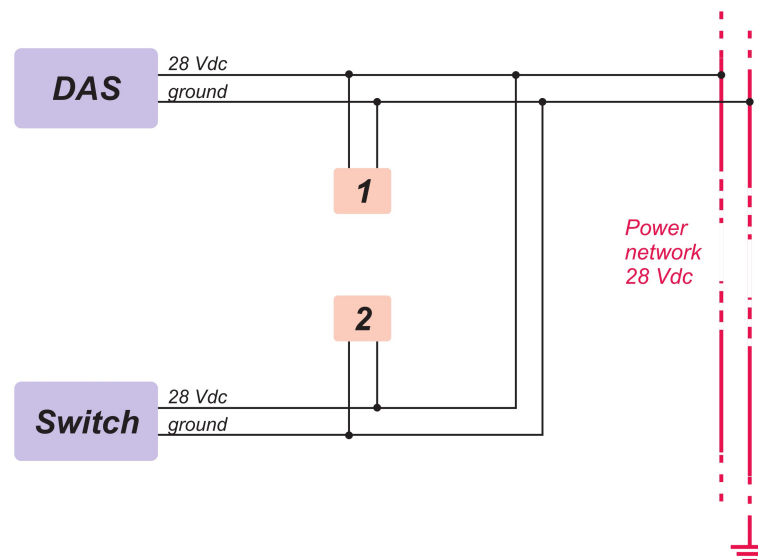
Figure 4: Illustration of the measurement configuration CF #2.

transmit the data via Ethernet interface to a switch that deliveries it to a pair of PLC modems. Then, the received data is sent to a PC. In this situation, CF #2 is adopted in order to measured CFR, additive noise, and access impedance estimates for the PLC channel. Figure 4 illustrates the block diagram for CF #2, such that the blocks #1 and #2 represent the PLC modems. This configuration is an option of harness topology to facilitate both data communication and energy delivery based on CM signal propagation. In addition, the CF #2 can alleviate the multipath effect, since it is used one physical defined path to connect both PLC modems and instrumentations equipments.

It is important to highlight that in both measurement configurations, the grounds are connected to the aircraft's chassis. It means that CM propagation is adopted.

3.1.1 Channel Frequency Response

We used the method presented in [43] to obtain estimates of CFR. The main advantage of this method over the traditional one[1] is that we can have a CFR estimate every 23.04 μs and this estimation period can be easily changed if it is necessary, since it is based on OFDM scheme.

To obtain the measured data, the measurement setup is connected to the power lines as in Fig. 5. In that case, the measurement setup is constituted by the following components:

- E10-P (Figure 6a): It is a portable rubidium frequency reference device used to generate a clock frequency signal reference with high accuracy for the signal generator.

- CompuGen 4300 (Figure 6d): It is an arbitrary waveform generator board installed into a rugged computer (Figure 6b). In order to operate, a previously designed sounding sequence, which is provided by [43], is loaded into the memory of the board. In the following, the analog waveform associated with the sounding sequence stored in the memory is outputted through the output channel. Finally, this signal is injected into the electric power grid under analysis through the capacitive coupler.

- Capacitive PLC coupler: It is a circuit used to connect both waveform generator and waveform digitizer boards to the electric power grid (Figure 6f). Basically, it is applied to block the 28 Vdc signal from the power line and to limit the maximum frequency for operating the PLC system or for data acquisition or generation purposes.

- Razor CompuScope 1642 (Figure 6c): It is a waveform digitizer board installed into a rugged computer. Its function is to convert the analog signal into a discrete time sequence, which comprises the inject sounding signal distorted by the PLC channel defined between the arbitrary waveform generator and waveform digitizer boards. This discrete time sequence is used by [43] to estimate the CFR.

The measurement setup can be divided into two blocks (see Figures 2, 4, and 5), where the block #1 is responsible for injecting the sounding signal into the aircraft electric power grid while block #2 is responsible for collecting it.

As it is illustrated in Figure 5, the sounding signal is coupled with a power line through the waveform generator and it is collected by the waveform digitizer. The sounding signal is generated with a sampling frequency of 200 MHz while the received signal was sampled with a frequency equal to 250 MHz. Then, after the signal digitization, the

---

[1] The traditional method used to collect CFR estimates is the use of a VNA equipment, see Figure 6e.
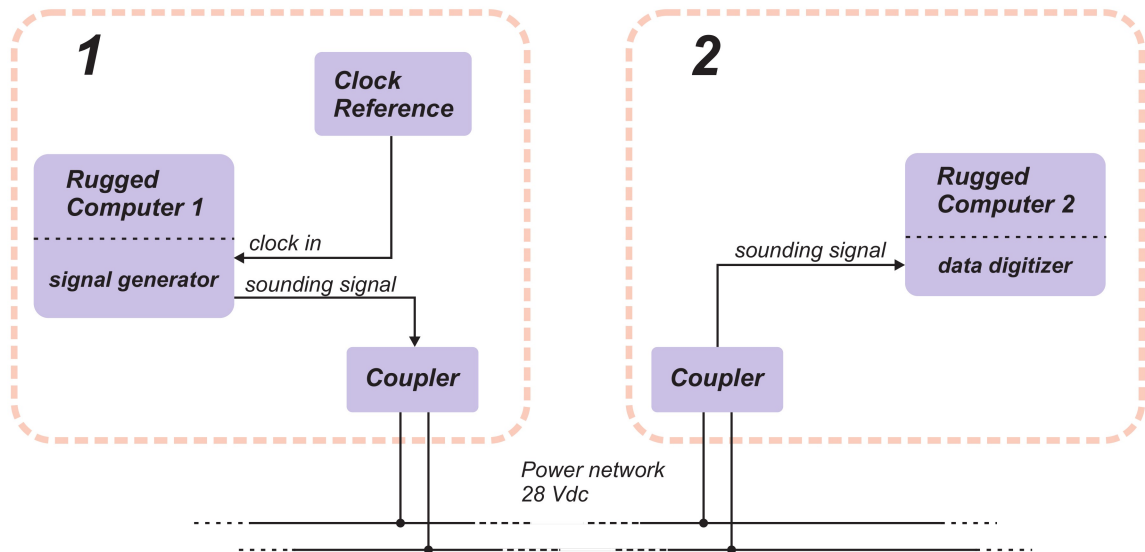
Figure 5: Block diagram of sounding-based measurement setup.

acquired sequence is resampled in order to obtain its version for the sampling frequency of 200 MHz. As depicted in Figure 7, the sequence is pre-processed through the following steps: first, upsampling with $L = 4$, then filtering by a low pass filter with cutoff frequency equal to π/L and, finally, downsampling with $M = 5$. In sequel, with the discrete-time version of both transmitted and pre-precessed received signals, the channel-estimation method described in [43] applies. This method encompasses the following stages: (i) input-output timing synchronization to estimate the start point of the sounding sequence; (ii) initial channel estimation to obtain the CFR estimates; (iii) sampling-frequency offset correction to avoid degradation of the CFR estimates due to difference between clocks of the transmitter and receiver; (iv) channel estimation enhancement, which reduces the additive noise presence. The parameters used for the channel estimation are summarized in Table 1. The sounding sequence is composed of consecutive OFDM symbols [49].

More details about the measurement procedure are presented in [50].

Table 1: Parameters of CFR estimation method.

Description	Value
Sampling frequency	$f_s = 200$ MHz
Number of sub-carriers	$N = 2048$
Modulation	BPSK
Cyclic prefix length	$L_{cp} = 512$
Frequency resolution	$\Delta_f = 48.83$ kHz
Symbol duration	$23.04 \ \mu$s

(a) E10-P portable rubidium frequency reference [44].

(b) Rugged computer [45].
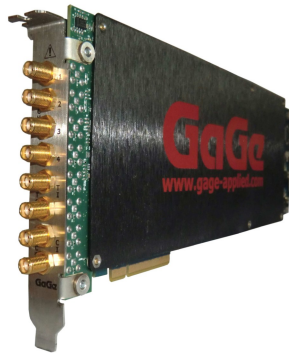
(c) Razor CompuScope 1642 waveform digitizer board [46].

(d) CompuGen 4300 waveform generator board [46].

(e) N9923A portable vector network analyzer [47].
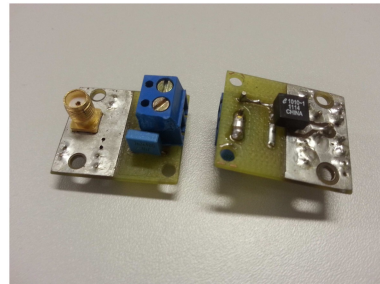
(f) Capacitive PLC couplers [48].

Figure 6: Equipments used in the measurement setups.
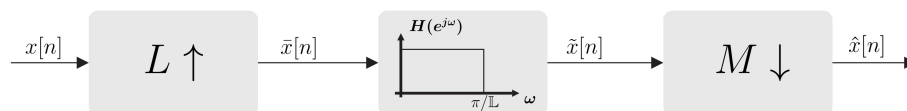
Figure 7: Block diagram of the signal resampling.

3.1.2   Additive Noise

Measurements of the additive noise were performed using the waveform digitizer and the capacitive PLC coupler (see Fig. 8). There was no sounding signal injected in the aircraft power grid, i.e., the waveform generator was turned off. Also, the noise signal

was recorded at the points where the blocks #1 and #2 are connected. The noise signal was sampled with a frequency of 250 MHz. However, the focus of the PSD analysis is on the frequency band $1.7 - 100$ MHz. Then, the sequence recorded was resampled by using the procedure showed in Figure 7. As a result, the resampled sequence correspond to the signal occupying the frequency band between 0 and 100 MHz.
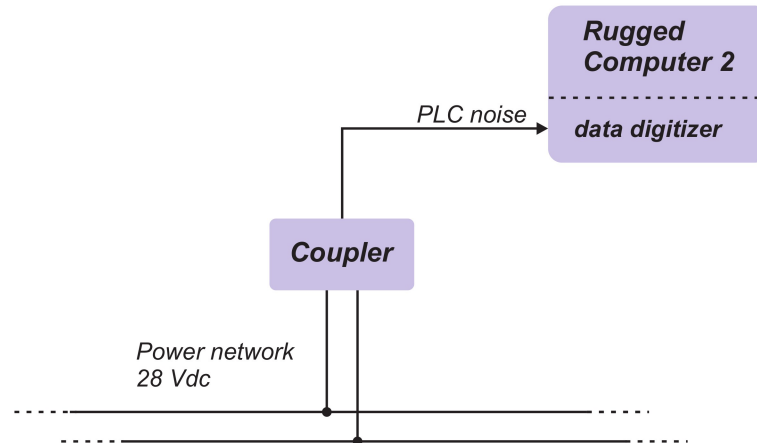
Figure 8: Block diagram of the measurement setup used to measure the additive noise.

3.1.3   Access Impedance

The access impedance was collected from block #1 and block #2 of both power lines measurement configurations through a VNA. The VNA adopted was the portable N9923A manufactured by Agilent Technologies company [47], see illustration in Figure 6e. The VNA comprises the frequency band $1.7 - 100$ MHz and was configured with the maximum resolution, which is 1001 points. The measurement was carried out using only one port of the VNA and, in addition, a capacitive coupler was used (see Fig. 9). It is important to emphasize that the capacitive coupler influence was removed through the calibration process of the VNA.
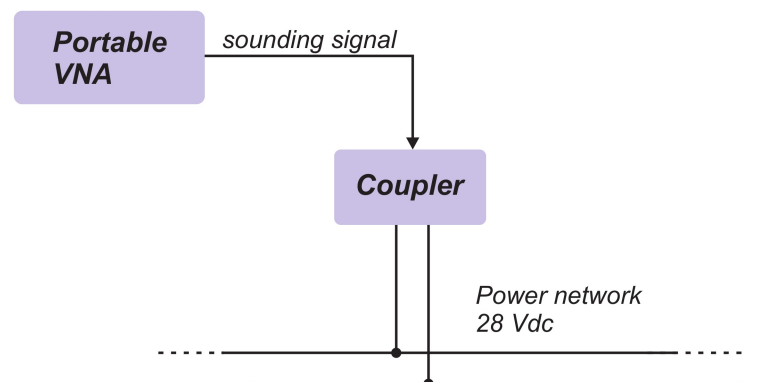
Figure 9: Block diagram of the measurement setup used to measure the access impedance.

3.2 Measurement Campaign

With the measurement configurations and setups described in Section 3.1, we carried out a measurement campaign in the electric power grid used to supply electric energy to the instrumentation of the flight test executive aircraft Legacy 450 (see Fig. 10). The aircraft was appropriate equipped to realize flight tests. As a precaution, the measurement campaign was carried out with the aircraft powered by an external power generator. During the measurement campaign, all instruments and equipments used in flight tests were powered on.

Figure 10: Executive aircraft Legacy 450 [1].

We collected $3,422$ and $3,446$ estimates of CFR for CF #1 and CF #2, respectively. Regarding the additive noise, three measures with 32×10^6 samples from each block were obtained, totalizing six measures for each power lines measurement configuration. Finally, considering the access impedance, three measures for CF #1 and seven measures for CF #2 ($1,001$ samples per measure) were collected.

It is important to emphasize that to get an available aircraft and enough time for the measurement campaign are not easy tasks to be accomplished. To carried out this measurement campaign, three days were needed at the facility of the aircraft manufacture.

3.3 Data Analysis

In this section we describe the performance metrics used to assess the data obtained in the measurement campaign. These metrics are important to understand the PLC channel behavior and, consequently, to support the design of novel PLC systems.

3.3.1 Average Channel Gain

The ACG is expressed by

$$\bar{G} = \frac{1}{B} \int_B |H(f)|^2 df, \tag{3.1}$$

where $H(f)$ is the channel frequency response and B is the frequency band. $\bar{G}$ is usually represented in decibel (dB) as $\bar{G}_{dB} = 10 \log \bar{G}$. However, the average channel attenuation (ACA), performed by $\bar{A}_{dB} = -\bar{G}_{dB}$, is adopted for the analyses presented in this paper.

ACA values can indicate the attenuation profile of a communication medium and, as consequence, can provide a rough estimate of channel capacity as well as the path loss.

3.3.2 Root Mean Squared Delay Spread

The RMS-DS is the transmitted power distribution over the paths in a multipath environment, and can be defined as the squared root of the second central moment of the power delay profile. For a channel impulse response (CIR), $h(t)$, the RMS-DS, τ_{rms}, is given by

$$\tau_{rms} = \sqrt{\frac{\int_0^\infty (t - \bar{\tau})^2 |h(t)|^2 dt}{\int_0^\infty |h(t)|^2 dt}}, \tag{3.2}$$

where

$$\bar{\tau} = \frac{\int_0^\infty t |h(t)|^2 dt}{\int_0^\infty |h(t)|^2 dt}. \tag{3.3}$$

The RMS-DS indicates how dispersive the communication channel is. This information is used to determine the guard interval duration in a multi-carrier modulation (i.e. OFDM and hermitian symmetric OFDM (HS-OFDM)) to avoid inter-symbol interference.

3.3.3 Coherence Time

The coherence time defines the interval time in which the CIR is considered time-invariant. Let a CIR of a PLC channel at instant t due to a unit impulse $\delta(\cdot)$ applied at the instant τ to be defined as

$$h(t, \tau) = \sum_{l=1}^{L} \alpha_l(t) \delta(t - \tau - \xi_l), \tag{3.4}$$

where L is the number of echoes of a transmitted signal arriving at the receiver; α denotes the zero mean complex gain that incorporates the attenuation factor and phase shift of the l-th echo; and ξ_l is the individual time delay. If $p(t)$ is the input of $h(t, \tau)$, its output is given by

$$p_o(t) = \int_{-\infty}^{\infty} h(t, \tau) p(\tau) d\tau = \sum_{l=1}^{L} \alpha_l(t) p(t - \xi_l) \tag{3.5}$$

In a time invariant linear channel the complex gains do not change with time. Thus, the coherence time of the channel modeled by (3.4) is related to the coherence time of the gains $\{\alpha_l(t)\}$. When the complex process $\alpha_l(t)$, $l = 1, 2, \ldots, L$ are uncorrelated and wide-sense stationary, i.e.

$$\mathbb{E}[\alpha_l(t_1)\alpha_k^*(t_2)] = 0, \quad l \neq k \tag{3.6}$$

and

$$\mathbb{E}[\alpha_l(t)\alpha_l^*(t+\Delta)] = R_{\alpha_l}(\Delta t), \quad l = 1, 2, \ldots, L, \tag{3.7}$$

the channel characterized in (3.4) is wide-sense stationary uncorrelated scattering (WSSUS).

The correlation index between the samples of $\alpha_l(t)$ for a Δt time unit is expressed as

$$\rho_{\alpha_l}(\Delta t) = \frac{R_{\alpha_l}(\Delta t)}{P_l}, \quad l = 1, 2, \ldots, L, \tag{3.8}$$

where $P_l = R_{\alpha_l}(0) = \mathbb{E}[|\alpha_l^2(t)|]$ is the average power of the l-th path.

The correlation index of a WSSUS channel described by (3.4) and (3.7) results as the weighted average of the individual correlation index $\rho_h(\Delta t)$ [15]:

$$\rho_h(\Delta t) = \frac{\sum_{l=1}^{L} P_l \rho_{\alpha_l}(\Delta t)}{\sum_{l=1}^{L} P_l}, \quad 0 \leqslant |\rho_h(\Delta t)| \leqslant 1. \tag{3.9}$$

Hence, the coherence time (Δt) of a channel can be obtained through

$$|\rho_h(\Delta t)| \geqslant \beta, \tag{3.10}$$

where $0 < \beta < 1$ is the correlation level admitted to consider the channel time-invariant during the time interval $\Delta t = T$. Thus in this context, the coherence time for a correlation level β is denoted by T_β if an OFDM scheme is applied, then T_β can be expressed as [15]

$$T_\beta = M_c(2N + L_{cp})T_s, \tag{3.11}$$

where M_c represents the number of consecutive CFR, which is obtained with an OFDM scheme, needed to reach a correlation level equal to β; N is the number of subchannels of one HS-OFDM symbol; L_{cp} denotes the length of the cyclic prefix; and T_s is the sampling period.

The knowledge of the coherence time is crucial for a communication system, since it indicates the periodicity in which the channel state information must be estimated to perform an effective equalization as well a resource allocation.

3.3.4 Coherence Bandwidth

The coherence bandwidth is the bandwidth where the CFR is considered to be flat. As in coherence time calculus, the channel is considered WSSUS and thus we assume that the correlation in a CFR depends only of the frequency spacing Δf. Therefore, the correlation index of a CFR is given by [10, 12]

$$R_H(\Delta f) = \int_B H(f)H^*(f + \Delta f)df, \quad 0 \leqslant R_H(\Delta f) \leqslant 1. \tag{3.12}$$

Hence, the coherence bandwidth can be estimated when

$$|R_H(\Delta f)| \geqslant \alpha |R_H(0)|, \tag{3.13}$$

where $0 < \alpha < 1$ is the lowest correlation level in which is admitted to characterize the channel with a coherence bandwidth of Δf.

Such characteristic can be used to choose the frequency bandwidth occupied by each subchannel in a multicarrier modulation, such as HS-OFDM and OFDM.

3.3.5   PSD of the Additive Noise

The PSD of additive noise is computed through the Welch method [51], which is based on the use of discrete Fourier transform (DFT). The Welch method was chosen is more suitable for estimating the PSD.

Let $\{v[n]\}_{n=0}^{N-1}$ be a vector constituted by N samples of a stationary, second-order stochastic sequence of the additive noise, in which for sake of simplicity $\mathbb{E}[v[n]] = 0$. This sequence is segmented into I sequences with length L. Then, the i-th segment $\{v_i[n]\} = \{v[n + (i-1)D]\}$ with $n = 0, 1, \ldots, L-1$ and $i = 0, 1, \ldots, I-1$. These segments can be composed of overlapping samples when $D < L$. For each segment of length L, it is calculated a modified periodogram from a sequence obtained from the product of the sequence $\{v_i[n]\}$ and a window $\{w[n]\}$, with $n = 0, 1, \ldots, L-1$, yielding the sequences $\{v_1[n]w[n]\}, \{v_2[n]w[n]\} \ldots \{v_I[n]w[n]\}$. The DFT for the i-th sequence is given by

$$V_i[k] = \frac{1}{L} \sum_{n=0}^{L-1} v_i[n]w[n]e^{-j2\pi ink/L}, \tag{3.14}$$

where $j = (-1)^{1/2}$. Finally, we obtain the I modified periodograms

$$P_i[l] = \frac{L}{U}|V_i[k]|^2, \; i = 1, 2, \ldots, I, \tag{3.15}$$

in which $l = k/L$, with $k = 0, \ldots, L/2$, since we assume that $\{L \in \mathbb{Z} \,|\, L$ even number$\}$, and $U = \frac{1}{L} \sum_{n=0}^{L-1} |w[n]|^2$. Finally, the PSD of the additive noise is given by

$$S[l] = \frac{1}{I} \sum_{i=1}^{I} P_i[l]. \tag{3.16}$$

3.3.6   Channel Capacity

By assuming that the PLC channel is linear, time invariant, and frequency selective and $x(t)$ and $v(t)$ are stationary and uncorrelated stochastic processes. Moreover, assuming that $v(t)$ is a colored Gaussian random process, then the channel capacity is given by [52]

$$C = \max_{S_x(f)} \int_B \log_2 \left(1 + \frac{S_x(f)|H(f)^2|}{S_v(f)} \right) df, \tag{3.17}$$

subject to $\int_B S_x(f)df \leq P_x$, in which B is the frequency band; $S_x(f)$ and $S_v(f)$ denote the PSD of the transmitted signal and the additive noise, respectively; $H(f)$ denotes the PLC CFR; and P_x is the total transmission power.

This is a relevant information to show the maximum data rate that a channel can offer.

3.4 Fit Evaluation

This section outlines the metrics used to choose a probability density function (pdf) from a set of pdfs applied to fit the relative frequency associated with the measured noise.

3.4.1 Log-Likelihood Function

Let $X_1, X_2, \ldots, X_n$ be random samples of some density $f(x; \boldsymbol{\theta})$, where $\boldsymbol{\theta} = [\theta_1, \ldots, \theta_j]^T$ is a set of j unknown parameters. Thus, the likelihood function can be defined as [53]

$$L(\boldsymbol{\theta}) = \prod_{i=1}^{n} f(x_i; \theta_1, \ldots, \theta_j), \tag{3.18}$$

and the log-likelihood function is given by

$$l(\boldsymbol{\theta}) = \sum_{i=1}^{n} \log f(x_i; \theta_1, \ldots, \theta_j). \tag{3.19}$$

Then, the maximum log-likelihood estimate, represented by the vector $\hat{\boldsymbol{\theta}}$, is obtained through

$$\hat{\boldsymbol{\theta}} = \arg\max_{\boldsymbol{\theta}} l(\boldsymbol{\theta}). \tag{3.20}$$

3.4.2 Information Criteria

Based on [13, 54–56], we choose the log-likelihood function and the information criteria Akaike information criterion (AIC), Bayesian information criterion (BIC), and efficient determination criterion (EDC) in order to determine the suitability of a probability distribution to model the relative frequency associated with the random samples. These criteria have the form

$$-2l(\hat{\boldsymbol{\theta}}) + Kc_n, \tag{3.21}$$

where $l(\cdot)$ is the log-likelihood function (3.18), K is the number of parameters that have to be estimated under the model, and c_n is the penalty term. We have $c_n = 2$ for AIC, $c_n = \log n$ for BIC, and $c_n = 0.2\sqrt{n}$ for EDC, in which n is the sample size. Observing (3.21), we can note that a compensation term Kc_n is added to the log-likelihood value, which penalizes the number of distribution parameters in order to provide a fair fitting assessment. For the log-likelihood function, the best modeling is the distribution that achieves the maximum log-likelihood value, whereas for the information criteria, the best modeling is the one that achieves minimum AIC, BIC, and EDC values.

3.5 Summary

This chapter presented the measurement configurations and setups used to collect CFR, additive noise, and access impedance estimates from the aircraft 28 Vdc electric power grid. Also, it described the measured campaign and the parameters used to analyze the raw data set.

4 Numerical Results

This chapter addresses the characterization of 28 Vdc electric power grid designed to supply instrumentation equipments in a fight test aircraft. This characterization is based on analyses of frequency response magnitude, ACA, coherence bandwidth, RMS-DS, coherence time, channel capacity, additive noise, and access impedance. Three distinct frequency bands are considered for the analyses: FB1, $1.7 - 30$ MHz, to comply with the European regulations for broadband PLC; FB2, $1.7 - 50$ MHz, to comply with ANATEL regulations (Brazilian telecommunication regulation) for broadband PLC [57]; and FB3, $1.7 - 100$ MHz, which is under investigation for addressing a new PLC regulation.

4.1 Channel Frequency Response

Figures 11 and 12 depict some interesting features about the aircraft PLC channel magnitude frequency response, considering the FB3 frequency band, which cover the other frequency bands, for CF #1 and CF #2, respectively. According to these plots, one can see maximum, minimum, and mean values of the channel magnitude frequency response. In Figure 11, the minimum values of magnitude attenuation are between 19.31 and 44.32 dB, whereas the maximum attenuation is higher than 100 dB. The mean values of magnitude attenuation are between 21.26 and 55.45 dB. Regarding CF #2, the channel magnitude frequency response shows a smooth decrease as the frequency increases, see Figure 12. Also, the minimum attenuation is between 10.09 and 30.43 dB, whereas the maximum attenuation can reach 78.19 dB. The mean values of the magnitude attenuation are between 10.46 and 39.86 dB.
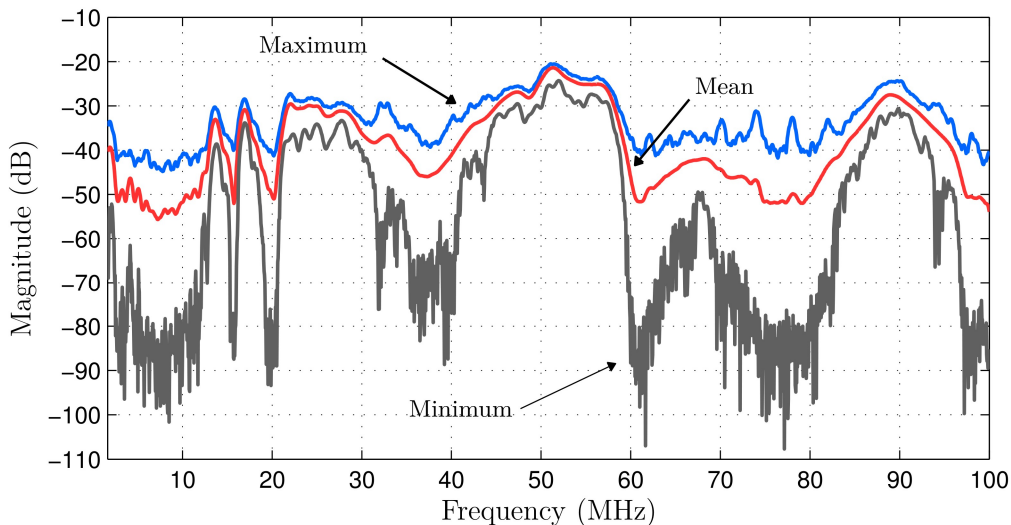
Figure 11: Aircraft PLC channel magnitude frequency response for CF #1.
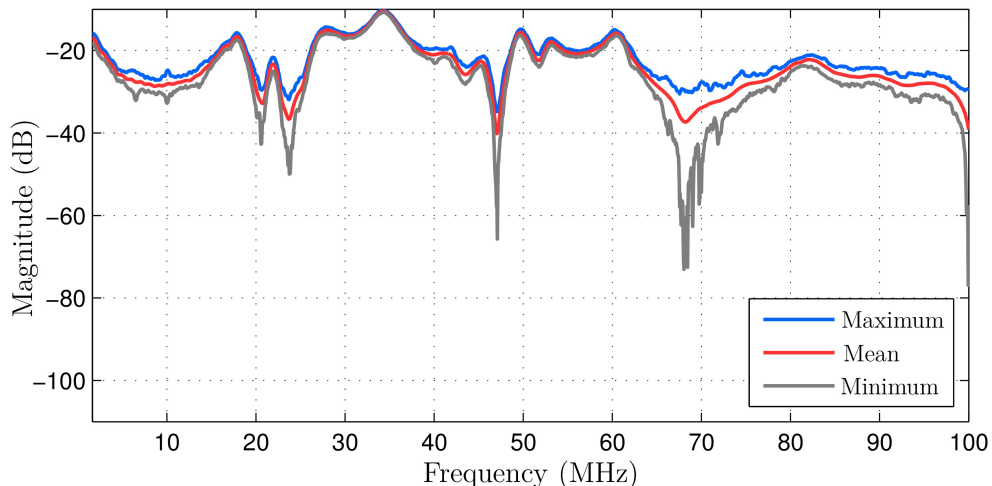
Figure 12: Aircraft PLC channel magnitude frequency response for CF #2.

Figure 13 shows the empirical cumulative distribution function (cdf) of the aircraft PLC channel magnitude frequency response considering FB1, FB2, and FB3 frequency bands for both measurement configurations. Observing the curves, we can note that, for both measurement configurations and disregarding the frequency bands, the magnitude attenuation behavior does not varies significantly. However, CF #2 shows attenuation levels lower than CF #1. For instance, if we take into account FB1 frequency band, a difference around 25 dB of attenuation for probabilities less than 0.15, 20 dB for probabilities between 0.5 and 0.35, and 12 dB for probabilities between 0.8 and 0.6 can be noted. It is worth to state that similar results were obtained for FB2 and FB3 as well.

Finally, based on the results presented in this section, we can note that CF #2 comes up as the best choice for data communication. The results presented in the following section will confirm such observation.
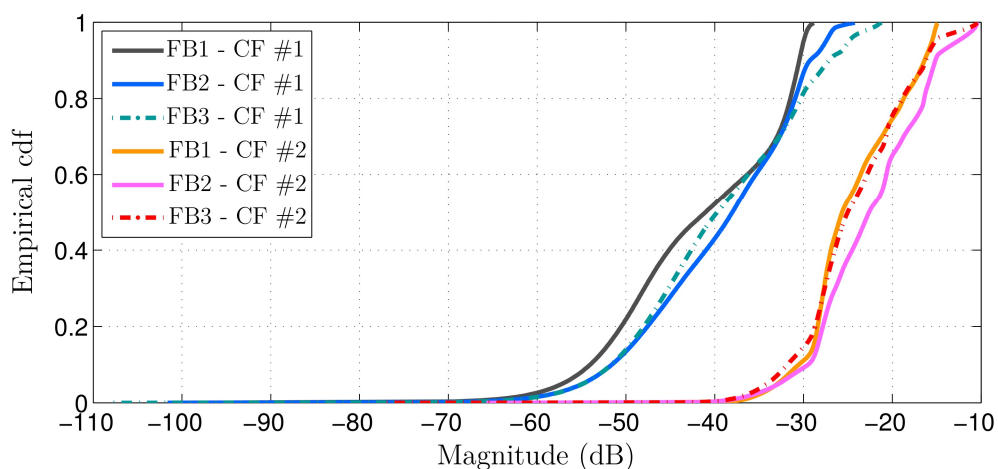
Figure 13: Empirical cdf of Aircraft PLC channel magnitude frequency response considering FB1, FB2, and FB3 frequency bands for both measurement configurations.

4.2 Average Channel Attenuation

ACA values of the measured aircraft PLC channels for both measurement configurations are summarized in Table 2.

Table 2: ACA for FB1, FB2, and FB3 frequency bands.

		Maximum	Mean	Minimum	Standard deviation
		Average Channel Attenuation (dB)			
CF #1	FB1	41.28	41.53	39.66	0.47
	FB2	43.64	39.32	38.02	0.35
	FB3	42.99	39.39	37.96	0.42
CF #2	FB1	25.3	24.42	24.01	0.12
	FB2	22.95	22.54	22.2	0.08
	FB3	24.64	24.24	23.51	0.17

Considering CF #1 and FB1 frequency band, maximum, mean, and minimum values of ACA found in aircraft PLC channels are 41.3, 41.5, and 39.7 dB, respectively, whereas in FB2 frequency band are 43.6, 39.3, and 38 dB. Finally, in FB3 frequency band, the ACA values are 43, 39.4, and 38 dB.

Analyzing FB1 frequency band, the difference between CF #1 and CF #2 for mean ACA is around 17.1 dB, whereas for maximum and minimum ACA values can reach 21 dB and 15.6 dB, respectively. Taking into account FB2 frequency band, the difference found for maximum, mean, and minimum ACA values are around 20.7, 16.8, and 15.8 dB, respectively. Finally, for FB3 frequency band, the difference of mean ACA is 15.1 dB, whereas for maximum and minimum values are 18.3 and 14.4 dB, respectively. Comparing the aforementioned values with those from CF #1, a significant decrease of ACA for the three frequency bands can be noted in favor of CF #2. Based on Table 2, ACA values indicate CF #2 as the best choice for data communication.

To compare ACA values obtained from the aircraft with those measures obtained from Brazilian in-home PLC channels [13], the FB2 frequency band is taken into consideration, since it is the frequency band regulated in Brazil for PLC system. While maximum, mean, and minimum ACA values measured in Brazilian in-home PLC channels were around 52.62, 25.24, and 9.98 dB, respectively, for aircraft PLC channels they are around 43.64, 39.32, and 38.02 dB for CF #1, and 22.95, 22.54, and 22.2 dB for CF #2. The results show that the ACA for CF #2 has, in average, a similar behavior to the Brazilian in-home PLC channels.

Table 3: PLC channel coherence bandwidth for FB1, FB2 and FB3 frequency bands.

			Coherence bandwidth (kHz)			
			Maximum	Mean	Minimum	Standard deviation
CF #1	FB1	B_{05}	11.17×10^3	3.94×10^3	2.05×10^3	2.05×10^3
		B_{07}	2.00×10^3	1.23×10^3	780.49	251.96
		B_{09}	634.15	495.50	390.24	48.44
	FB2	B_{05}	8.25×10^3	4.49×10^3	2.54×10^3	1.67×10^3
		B_{07}	3.71×10^3	2.18×10^3	1.07×10^3	830.8
		B_{09}	976.56	567.48	390.62	118.41
	FB3	B_{05}	6.88×10^3	6.39×10^3	5.81×10^3	131.32
		B_{07}	4.29×10^3	3.75×10^3	2.93×10^3	146.61
		B_{09}	1.51×10^3	1.26×10^3	634.77	94.42
CF #2	FB1	B_{05}	2.00×10^3	1.89×10^3	1.80×10^3	44.29
		B_{07}	1.27×10^3	1.19×10^3	1.12×10^3	30.43
		B_{09}	585.37	540.91	536.59	13.87
	FB2	B_{05}	6.54×10^3	6.26×10^3	5.91×10^3	131.26
		B_{07}	2.68×10^3	2.59×10^3	2.49×10^3	33.76
		B_{09}	1.17×10^3	1.08×10^3	976.56	32.97
	FB3	B_{05}	7.23×10^3	6.96×10^3	6.64×10^3	63.4
		B_{07}	3.22×10^3	2.98×10^3	2.73×10^3	57.92
		B_{09}	1.27×10^3	1.16×10^3	1.07×10^3	23.31

4.3 Coherence Bandwidth

The coherence bandwidth measured in aircraft PLC channels for both measurement configurations are summarized in Table 3, where B_{05}, B_{07}, and B_{09} refer to the correlation levels of 0.5, 0.7, and 0.9, respectively.

Regarding CF #1 and taking into account FB1 frequency band, the mean value of coherence bandwidth for B_{05} is around 3.94 MHz. It decreases to 1.23 MHz and 495.5 kHz when B_{07} and B_{09} are adopted, respectively. Comparing both measurement configurations, we can note that the coherence bandwidth found in CF #1 is slightly higher for B_{05} and B_{07} and lower for B_{09}.

Assuming B_{09}, since it is the value considered in literature to characterize the coherence bandwidth [10–13,58], and comparing the mean coherence bandwidth obtained from Brazilian in-home PLC channels (644.29 kHz) [13] with the ones found in aircraft PLC channels, differences among them are around 148.79 kHz and 103.38 kHz for CF #1 and CF #2, respectively.

According to Table 3, one can see that, for each measurement configuration, the coherence bandwidth increases as the frequency bandwidth increases. Taking a look at the Brazilian in-home PLC channels [13], we note that the mean coherence bandwidth for FB2 and FB3 are 750.55 kHz and 780.27 kHz, respectively, which is an indication that aircraft PLC channels are more frequency selective than Brazilian in-home PLC channels for FB1 and FB2. In contrast, for FB3, the aircraft PLC channels has the CFR planner than Brazilian ones.

4.4   Root Mean Squared Delay Spread

RMS-DS values for both measurement configurations are summarized in Table 4. Taking into account FB1 frequency band, the mean RMS-DS observed in CF #1 is 0.17 μs, whereas in CF #2 it is around 0.12 μs. For FB2, the mean RMS-DS values are 0.14 and 0.08 μs for CF #1 and CF #2, respectively. Finally, considering FB3, we have a mean RMS-DS equal to 0.07 μs for CF #1 and equal to 0.06 μs for CF #2. These results indicate that CF #1 has stronger signal reflections (higher multipath effects) than CF #2.

Note that mean RMS-DS values obtained from Brazilian in-home PLC channels [13] were around 0.15, 0.14, and 0.13 μs for FB1, FB2, FB3 frequency bands, respectively. Observing FB1 for both measurement configurations and FB2 for CF #1, the mean RMS-DS found in aircraft PLC channels has a behavior similar to the mean RMS-DS obtained from Brazilian in-home ones. However, analyzing FB2 for CF #2 and FB3 for both measurement configurations, the mean RMS-DS values estimated from aircraft PLC channels are much lower than the Brazilian in-home ones. Based on these results, we can state that the signal reflections are less presented in the aircraft electric power grid. Also, for FB2 (CF #2) and FB3 (CF #1 and CF #2) frequency bands, we can have a cyclic prefix length smaller than showed for the Brazilian in-home PLC channels and, as consequence, the bit rate of the aircraft PLC system based on OFDM scheme is higher than the in-home PLC system.

Table 4: PLC channel RMS-DS for FB1, FB2, and FB3.

RMS-DS (μs)					
		Maximum	Mean	Minimum	Standard deviation
CF #1	FB1	0.26	0.17	0.12	0.02
	FB2	0.22	0.14	0.09	0.02
	FB3	0.13	0.07	0.05	0.01
CF #2	FB1	0.14	0.11	0.09	0.01
	FB2	0.09	0.08	0.06	0.01
	FB3	0.07	0.06	0.06	0.001

Table 5: PLC channel coherence time for FB1, FB2, and FB3.

			Coherence time (ms)			
			Maximum	Mean	Minimum	Standard deviation
CF #1	FB1	T_{85}	2.81	1.4	0.14	1.06
		T_{90}	2.58	1.21	0.11	0.98
		T_{95}	2.33	0.61	0.02	0.68
		T_{99}	0.02	0.02	0.02	0
	FB2	T_{85}	2.58	0.98	0.11	0.89
		T_{90}	2.58	0.87	0.09	0.88
		T_{95}	2.28	0.64	0.05	0.72
		T_{99}	0.02	0.02	0.02	0
	FB3	T_{85}	2.58	0.83	0.09	0.88
		T_{90}	2.58	0.74	0.07	0.83
		T_{95}	2.58	0.58	0.05	0.78
		T_{99}	0.11	0.04	0.02	0.03
CF #2	FB1	T_{85}	10.68	6.62	2.56	4.24
		T_{90}	10.68	6.61	2.42	4.25
		T_{95}	10.68	6.57	2.14	4.25
		T_{99}	10.68	5.75	0.97	3.86
	FB2	T_{85}	10.67	6.59	2.4	4.24
		T_{90}	10.67	6.56	2.14	4.25
		T_{95}	10.67	6.41	1.66	4.2
		T_{99}	10.67	5.35	0.71	3.72
	FB3	T_{85}	10.67	6.54	1.91	4.27
		T_{90}	10.67	6.43	1.66	4.22
		T_{95}	10.67	6.09	2	4.05
		T_{99}	10.67	5.12	0.48	3.73

4.5 Coherence Time

The results of coherence time measured in aircraft PLC channels for both measurement configurations are summarized in Table 5, where T_{85}, T_{90}, T_{95}, and T_{99} refer to the correlation levels of 0.85, 0.90, 0.95, and 0.99, respectively. In Table 5, the results show that coherence time values decrease as the correlation level rises independently of frequency bands and measurement configurations, which is expected. Furthermore, coherence time values decrease as the frequency band increases in both measurement configurations.

Taking into account FB1 frequency band and T_{90}, since such correlation level is used in literature to characterize the PLC channel [11, 15, 58], the maximum, mean, and minimum coherence time values observed in CF #1 are around 2.58, 1.21, and 0.11 ms, respectively, whereas for CF #2 are 10.68, 6.61, and 2.42 ms. Regarding FB2 and FB3 frequency bands, the coherence time values are very similar, except the mean values for CF

#1 which are 0.87 and 0.74 ms for FB2 and FB3, respectively. Comparing the estimates of coherence time from both measurement configurations, the CIR obtained from CF #2 varies very slowly when compared to CF #1 and the Brazilian in-home PLC channels, where the maximum coherence time is 1.75 ms. Based on these coherence time estimates, the periodicity in which the channel state information must be estimated in an aircraft PLC system based on OFDM scheme is smaller than in the Brazilian in-home counterpart, which means that the bit rate in aircraft PLC systems is higher than in the in-home ones.

4.6 Additive Noise

Figures 14 and 15 depict the CSD of the additive noise measured in flight test aircraft power lines for CF #1 and CF #2, respectively. CSD was chosen rather than the PSD since the aeronautic standard RTCA/DO-160G [20] gives the upper limit (20 dBμA/kHz) of the signal in terms of CM current flowing on all cables. For the sake of simplicity, only FB3 frequency band was adopted in the analysis since FB3 cover all the other frequency bands.

In Figure 14, the CSD varies from -14 dBμA/kHz (-110.5 dBm/Hz, impedance of 50 Ω) up to 23 dBμA/kHz (-80 dBm/Hz, impedance of 50 Ω). Figure 15 shows a similar behavior; however, the mean CSD yields a slight higher oscillation than the mean CSD found in the CF #1.
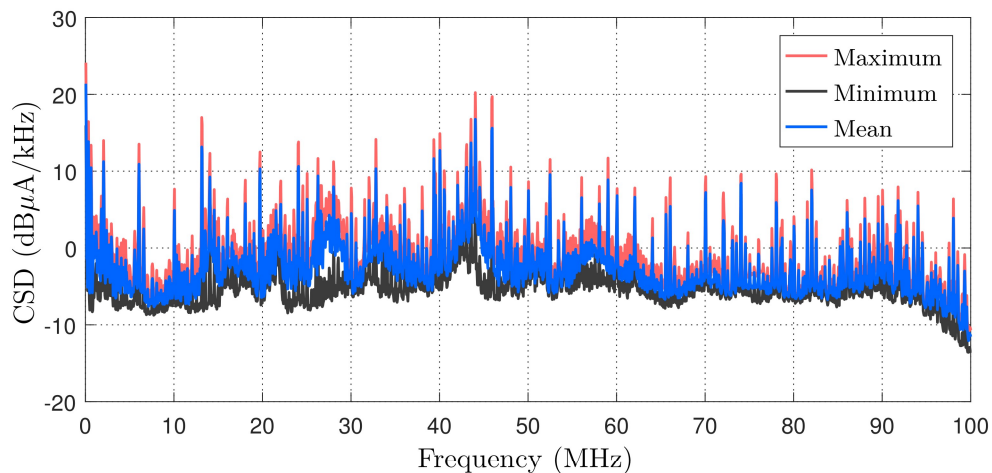
Figure 14: The CSD of the measured noise in CF #1.

Figure 17 shows a measured of the additive noise in time domain considering the FB3 frequency band for CF #2. Observing the figure, we can note the presence of three noise components: colored background noise, impulsive component #1, and impulsive component #2. The impulsive components #1 and #2 are highlighted by the red and blue envelopes, respectively, in Figure 17. A periodicity is noticed in component #1, whereas, apparently, the component #2 is aperiodic. Besides, it is likely that both impulsive noise

Figure 15: The CSD of the measured noise in CF #2.

components were generated by switched power supplies from the external power generator that powered the aircraft during the measurement campaign.

Figure 16: Time domain sample of the measured noise in CF #1.

Figure 17: Impulsive components of the measured noise in CF #1.

Figure 18 illustrates the impulsive events of the component #1 highlighted in Figure 17 with the characteristic parameters amplitude $A = \max\{A_i^+, A_i^-\}$, width $t_{w,i}$, and arrival t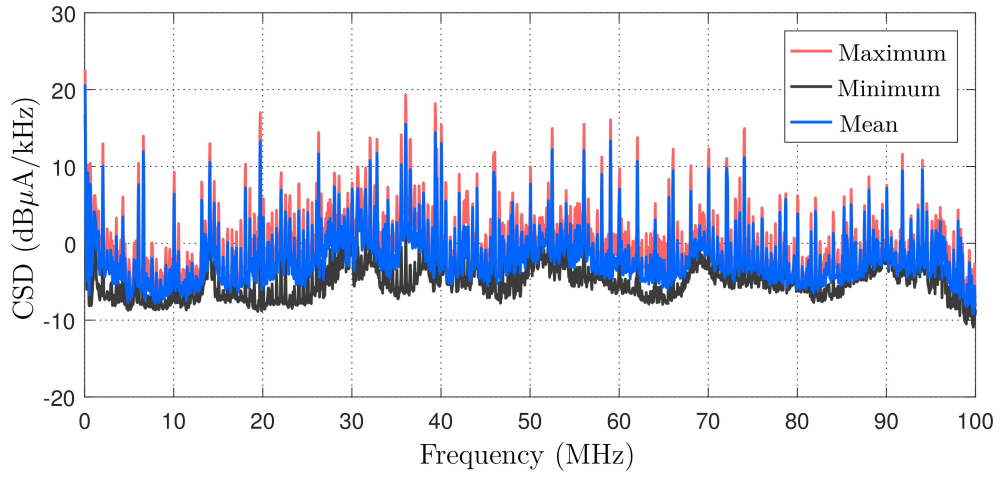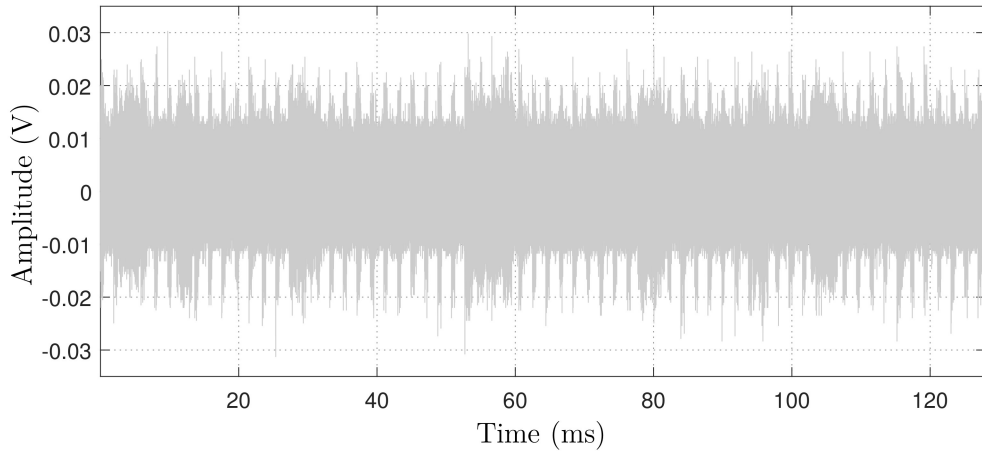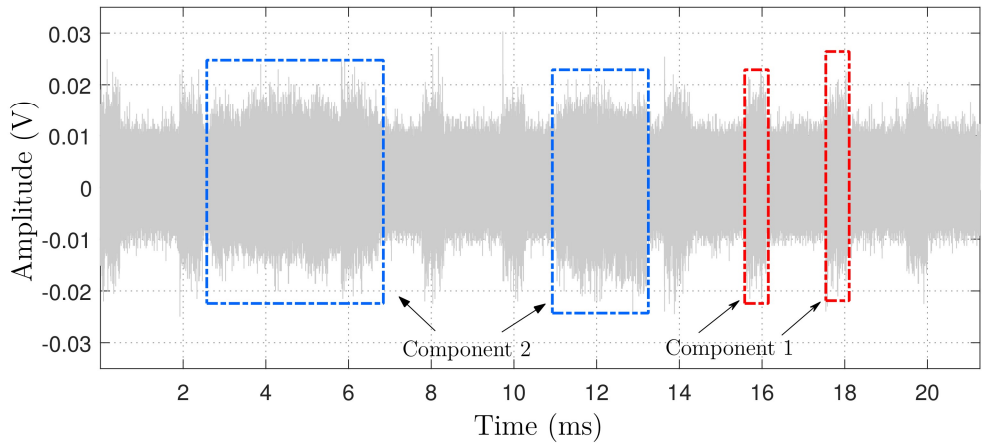ime $t_{arr,i}$. The interval between two consecutive impulses is represented by the inter-arrival time t_{IAT} or the interval t_d, where [59]

$$t_{IAT} = t_{w,i} + t_d = t_{arr,i+1} - t_{arr,i}, \tag{4.1}$$

such that i denotes the ith impulse.
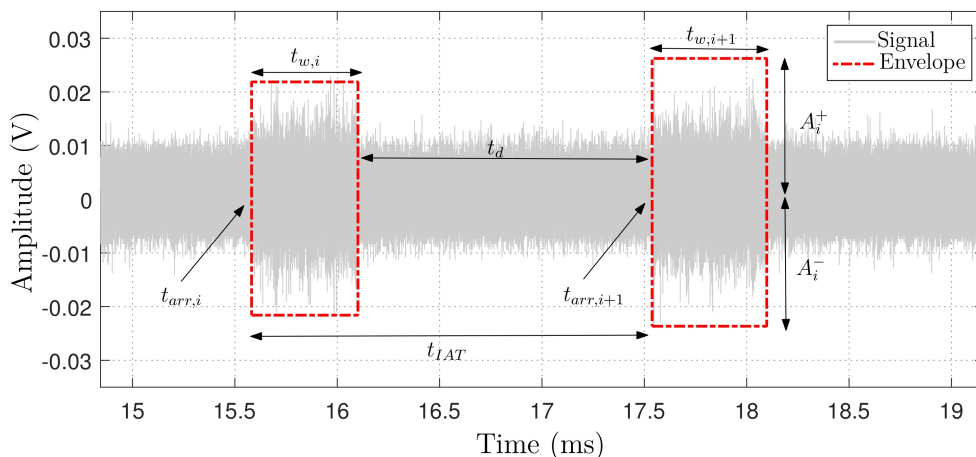
Figure 18: Illustration of parameters used to characterize impulsive noise components.

Tables 6 and 7 summarize the statistical estimates of t_{IAT}, t_w, and power for the impulsive components #1 and #2, respectively. Taking CF #1 into account, we can note that the impulsive component #1 has a mean t_{IAT} equal to 1.91 ms, a mean t_w equal to 0.437 ms, and a mean power of -19.17 dBm. Regarding CF #2, the mean inter-arrival time, t_{IAT}, is 1.30 ms higher and mean t_w is 0.339 ms lower than CF #1. Besides that, CF #2 has a mean power of -13.48 dBm, which is more than double the CF #1.

In Table 7, for the impulsive component #2, the mean values of t_{IAT}, t_w, and power are 3.96 ms, 16.9 ms, and -18.24 dBm for CF #1, respectively. Comparing both measurement configurations, no significative difference is observed. Also, comparing both impulsive components, CF #2 is worst than CF #1 for data communication.

4.6.1 Fitting Evaluation

In order to obtain a suitable statistical model for aircraft PLC noise in FB1, FB2, and FB3 frequency bands, some symmetric continuous distribution were taken into account. The considered symmetric distributions adopted in the analysis were Bernolli-Gaussian, Logistic, Normal, and t Location-Scale. It is important to state that the parameters for Logistic, Normal, and t Location-Scale distributions were estimated through the maximization of the log-likelihood function (3.20) described in Chapter 3. On the

Table 6: Parameters of the measured impulsive component #1.

	Parameter	Maximum	Mean	Minimum	Standard deviation
Impulsive Component #1					
CF #1	t_{IAT} (ms)	2.49	1.91	0.347	0.246
	t_w (ms)	1.55	0.437	3.48×10^{-3}	0.181
	Power (dBm)	-17.75	-19.17	-19.71	-31.23
CF #2	t_{IAT} (ms)	3.91	3.21	0.38	1.08
	t_w (ms)	1.08	9.78×10^{-2}	3.6×10^{-5}	0.156
	Power (dBm)	-5.99	-13.48	-17.67	-15.27

Table 7: Parameters of the measured impulsive component #2.

	Parameter	Maximum	Mean	Minimum	Standard deviation
Impulsive Component #2					
CF #1	t_{IAT} (ms)	25.6	16.9	7.66	6.98
	t_w (ms)	8.32	3.96	2.16	1.6
	Power (dBm)	-16.58	-18.24	-20.02	-23.51
CF #2	t_{IAT} (ms)	25.3	17.8	8.27	6.96
	t_w (ms)	7.08	3.99	2.12	1.59
	Power (dBm)	-17.37	-17.77	-18.24	-29.96

other hand, for Bernoulli-Gaussian distribution, the algorithm addressed in [60] was used, since its results showed good accuracy for parameters estimation.

Based on [55], log-likelihood function, AIC, BIC, and EDC were considered to quantify the suitability of chosen statistical distributions to model the aircraft PLC noise. The latter three criteria penalizes the number of parameters in order to obtain a fair comparison, avoiding overfitting[1]. The best modeling is the one that achieves the maximum log-likelihood and the minimum AIC, BIC, and EDC.

Table 8 lists the results obtained of the considered statistical distributions for FB1, FB2, and FB3 frequency bands. In Table 8, the best results are in bold. Moreover, observing FB1 frequency band for CF #1 and CF #2 measurement configurations and FB2 for CF #1, Table 8 shows that the Logistic distribution is the one that fits best for the aircraft PLC noise data set, whereas the second better is the t Location-Scale. On the other hand, when the FB2 for CF #2 and FB3 for CF #1 and CF #2 are taken into account, t Location-Scale is the one that fits best the aircraft PLC noise data set, whereas the second better is the Logistic distribution. Parameters from the two best statistical distributions for both measurement configurations considering all analyzed frequency bands are summarized in Appendix A - Table 9.

---

[1] Overfitting occurs when the statistical distribution are much complexity, such that having many parameters in relation to the observations. They overreacts to minor fluctuations describing either errors or noise instead of the analyzed data set.

Table 8: Evaluation Criteria for the aircraft PLC noise distributions.

		Distribution	Log-Likelihood	AIC	BIC	EDC
FB1						
CF #1		Bernoulli-Gaussian	224607398.67	−449214793.35	−449214762.06	−449212082.06
		Logistic	**229185391.94**	**−458370779.87**	**−458370748.58**	**−458368068.58**
		Normal	228619027.25	−457238050.49	−457238019.20	−457235339.20
		t Location-Scale	**229180367.70**	**−458360729.40**	**−458360682.47**	**−458356662.47**
CF #2		Bernoulli-Gaussian	227078798.78	−454157593.55	−454157562.26	−454154882.26
		Logistic	**232152448.24**	**−464304892.48**	**−464304861.19**	**−464302181.19**
		Normal	231284695.56	−462569387.13	−462569355.83	−462566675.84
		t Location-Scale	**232140713.61**	**−464281421.22**	**−464281374.29**	**−464277354.29**
FB2						
CF #1		Bernoulli-Gaussian	349339672.48	−698679340.96	−698679308.64	−698675839.53
		Logistic	**353736318.68**	**−707472633.36**	**−707472601.04**	**−707469131.93**
		Normal	352700039.66	−705400075.31	−705400043.00	−705396573.89
		t Location-Scale	**353721790.31**	**−707443574.62**	**−707443526.15**	**−707438322.48**
CF #2		Bernoulli-Gaussian	352413453.24	−704826902.49	−704826870.17	−704823401.06
		Logistic	**355711702.34**	**−711423400.68**	**−711423368.37**	**−711419899.26**
		Normal	355235117.02	−710470230.05	−710470197.74	−710466728.62
		t Location-Scale	**355801156.87**	**−711602307.73**	**−711602259.26**	**−711597055.60**
FB3						
CF #1		Bernoulli-Gaussian	668844687.34	−1337689370.68	−1337689336.98	−1337684417.26
		Logistic	**674921615.33**	**−1349843226.65**	**−1349843192.95**	**−1349838273.23**
		Normal	673125153.66	−1346250303.32	−1346250269.62	−1346245349.90
		t Location-Scale	**674938015.66**	**−1349876025.33**	**−1349875974.78**	**−1349868595.20**
CF #2		Bernoulli-Gaussian	657974812.85	−1315949621.70	−1315949588.00	−1315944668.28
		Logistic	**664860060.75**	**−1329720117.49**	**−1329720083.79**	**−1329715164.07**
		Normal	663912011.78	−1327824019.56	−1327823985.86	−1327819066.14
		t Location-Scale	**665051284.57**	**−1330102563.15**	**−1330102512.60**	**−1330095133.02**

Figures 19 and 20 plot the histograms of the aircraft PLC noise collected from CF #1 and CF #2 for FB1, respectively. Also, Figures 21 and 22 show the same for FB2 as well as Figures 23 and 24 for FB3. Besides, the two best statistical distribution models (Logistic and t Location-Scale) are plotted. Observing the figures, the symmetry is clearly noticed, as well as that the Logistic distribution model fits very well for both measurement configuration in FB1 (Figures 19 and 20) and for CF #1 in FB2 (Figures 21). On the other hand, the t Location-Scale distribution model fits very well for CF #2 in FB2 and for both measurement configurations in FB3 (Figures 23 and 24).

Finally, Table 8 shows that the Normal distribution offers the 3rd best fit for

modeling the additive noise. Since the difference between the three distributions is not relevant, the normality assumption for the additive noise is considered in Section 4.7 in order to evaluate the channel capacity.
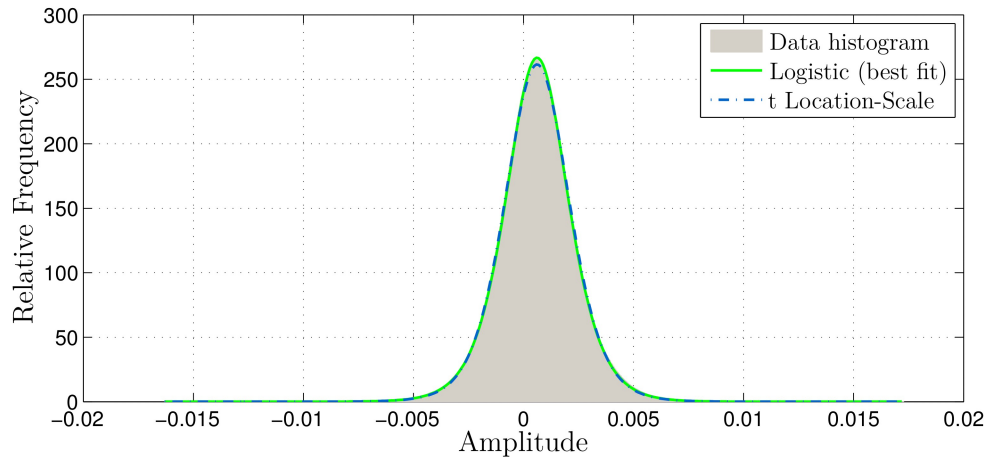

Figure 19: Histogram and distribution of additive noise for CF #1 considering FB1 frequency band.
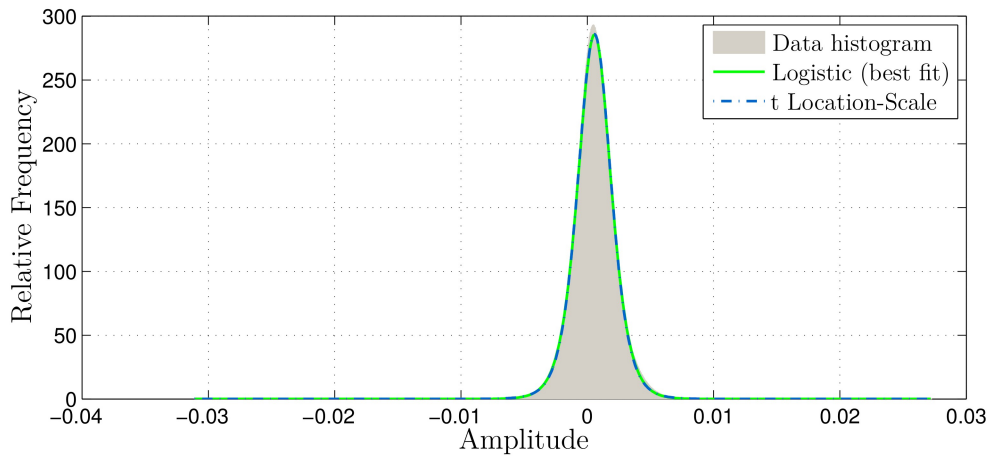

Figure 20: Histogram and distribution of additive noise for CF #2 considering FB1 frequency band.

Figure 21: Histogram and distribution of additive noise for CF #1 considering FB2 frequency band.

Figure 22: Histogram and distribution of additive noise for CF #2 considering FB2 frequency band.

4.7   Channel Capacity

The upper, lower, and mean channel capacities for FB1, FB2, and FB3 are shown in Figures 25 and 26 for CF #1 and CF #2, respectively. As explained in Subsection 4.6, the channel capacity is presented in terms of CSD instead of PSD. The CSD of the transmitted signal ranges from 13 dBμA/kHz (-90 dBm/Hz, impedance of 50 Ω) up to 53 dBμA/kHz (-50 dBm/Hz, impedance of 50 Ω). The channel capacity was computed with the additive noise and the CFRs obtained from the measurement campaign.

In Figure 25, the channel capacity can reach 552, 315, and 206 Mbps for FB3, FB2, and FB1 for a CSD of 53 dBμA/kHz, respectively. However, in compliance with the aeronautic standard RTCA/DO-160 [20], the upper bound of CSD that the transmitter can emit is 20 dBμA/kHz, which limits the channel capacity to 34, 21, and 15 Mbps for FB3, FB2, and FB1, respectively.
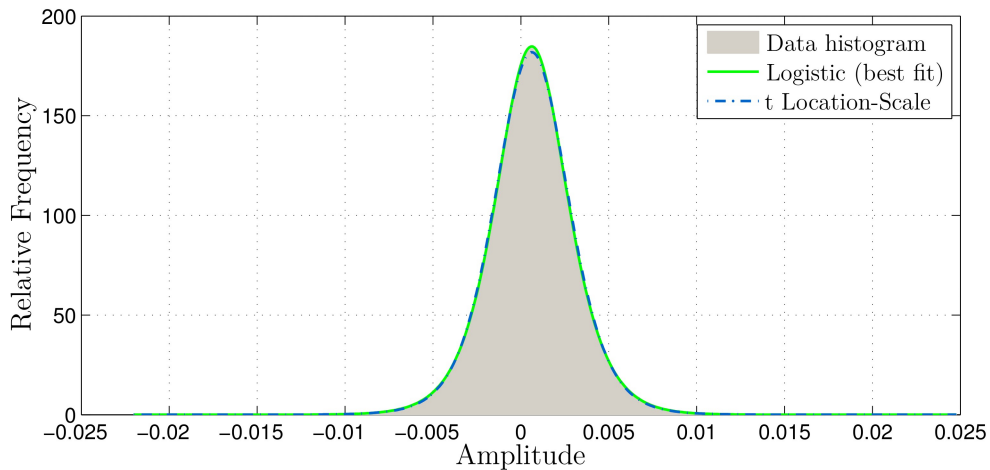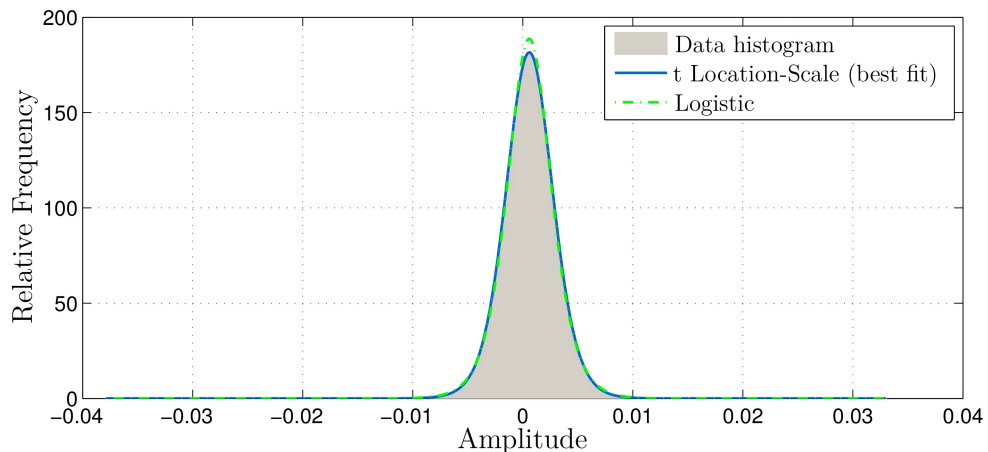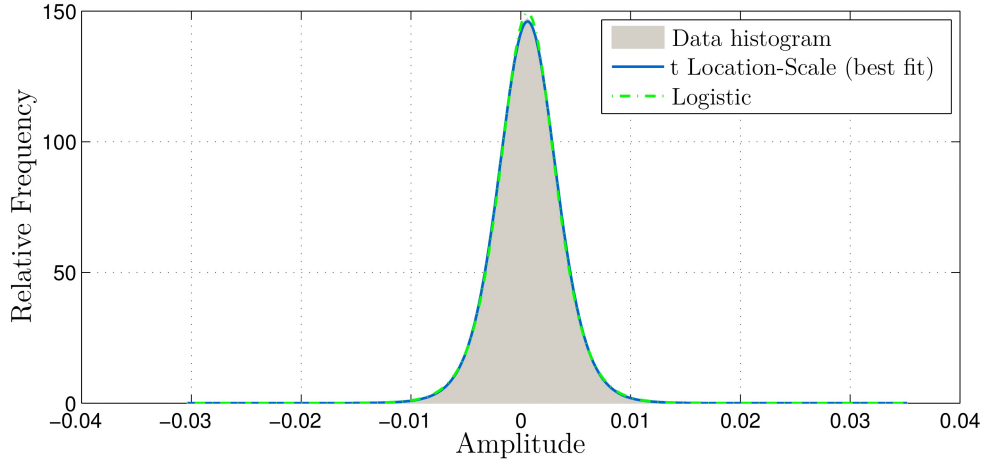
Figure 23: Histogram and distribution of additive noise for CF #1 considering FB3 frequency band.
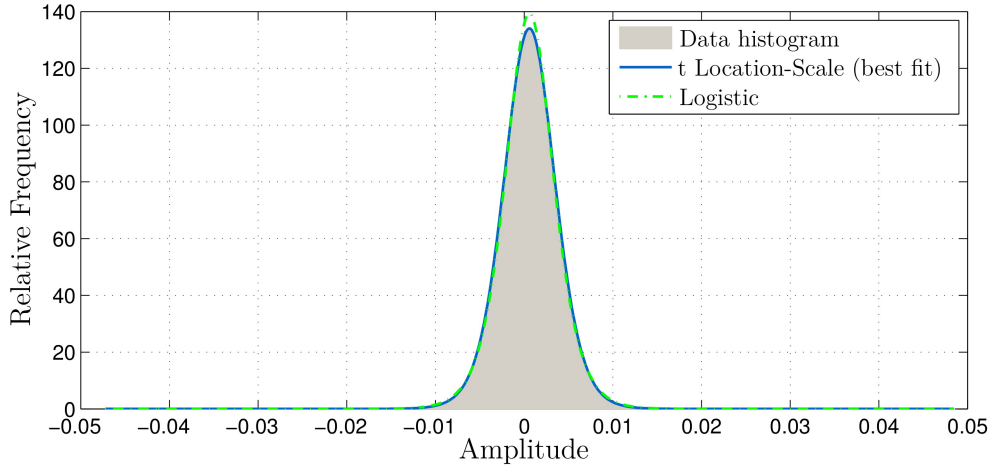
Figure 24: Histogram and distribution of additive noise for CF #2 considering FB3 frequency band.

Regarding CF #2 (Figure 26), we can note a small difference between upper, mean, and lower capacities when we compare to CF #1. Furthermore, its channel capacity can reach 988, 567, and 364 Mbps for FB3, FB2, and FB1, respectively. However, when the limit of aeronautic standard RTCA/DO-160 (20 dBμA/kHz that corresponds to) is applied, the channel capacities can only reach 100, 82, and 62 Mbps for FB3, FB2, and FB1, respectively.

Comparing the channel capacities of aircraft PLC channels for CF #2 with the ones obtained from Brazilian in-home PLC channels, which correspond to 1550, 800, and 450 Mbps for FB3, FB2, and FB1, respectively [13], when the CSD is −53 dBμA/kHz, differences of 892, 233, and 86 Mbps for FB3, FB2, and FB1 are observed, respectively. However, due to the limit of CM current flowing imposed by aeronautic standard RTCA/DO-160, this difference increases to 1450, 718, and 388 Mbps, respectively.
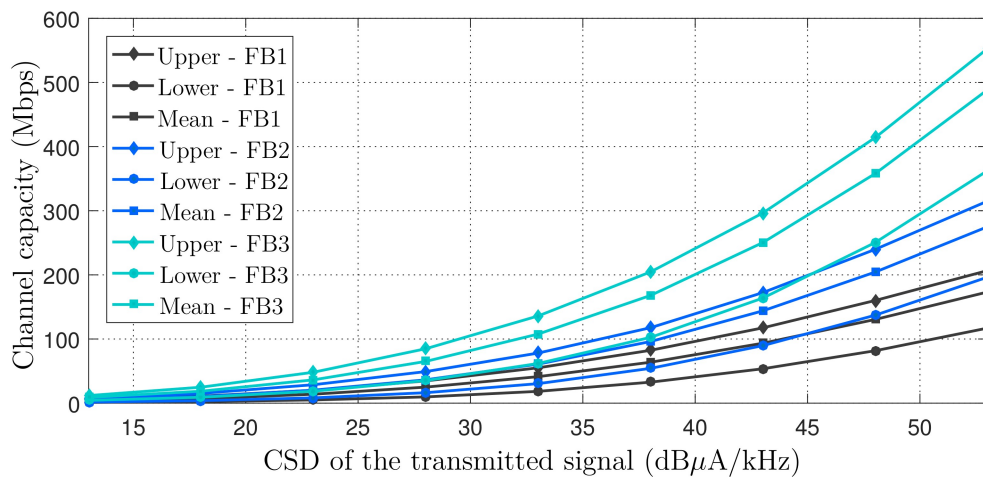
Figure 25: Channel capacity of the measured aircraft PLC channels for CF #1.
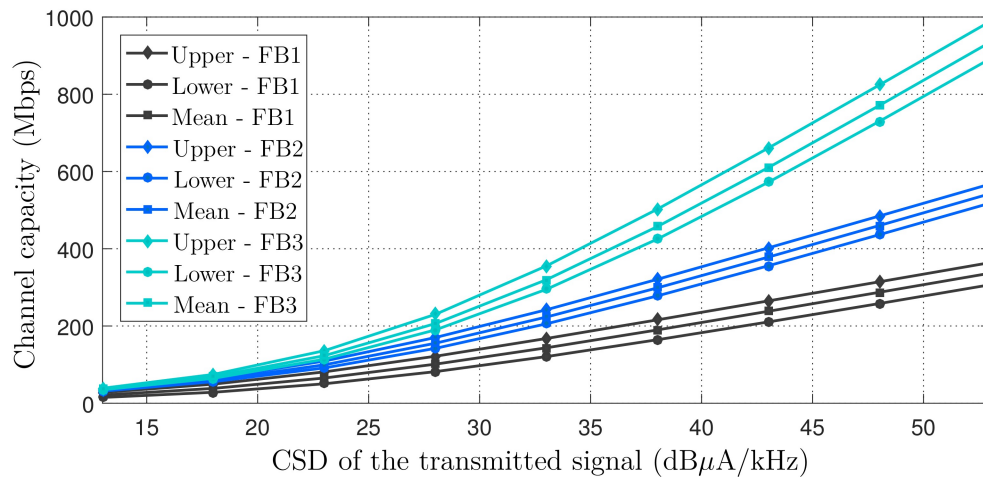
Figure 26: Channel capacity of the measured aircraft PLC channels for CF #2.

The obtained channel capacity results based on the constraints imposed by RTCA/DO-160 corroborates with previous works [8, 16–18]. According to these works, the PLC technology offers low data rate if CM propagation is adopted. The solution is to use a twisted pair (DM propagation) for decreasing the disturb noise and increasing the injected signal current.

However, as stated in [8], if a change in aeronautic standard is adopted in the future, so that the upper bound of CM current would increase to 40 dBμA/kHz, then channel capacities considering FB3, FB2, and FB1 will increase to 240, 139 and 96 Mbps for CF #1 and 565, 352, and 235 Mbps for CF #2, respectively.

4.8   Access impedance

Figures 27a and 27b illustrate real (resistive) and imaginary (reactive) components of the measured aircraft access impedance in CF #1. Fig 27a shows tree picks at frequen-

cies 13, 21, and 38 MHz, whose maximum resistive values found are 4.1, 2.5, and 8.1 kΩ, respectively. In Figure 27b, the reactive component reaches 5 kΩ in the maximum curve and −8.5 kΩ in the minimum curve at frequency 13 MHz. Furthermore, at frequency 38 MHz, the maximum reactance reaches 4 kΩ, whereas the minimum is as low as −4.2 kΩ.
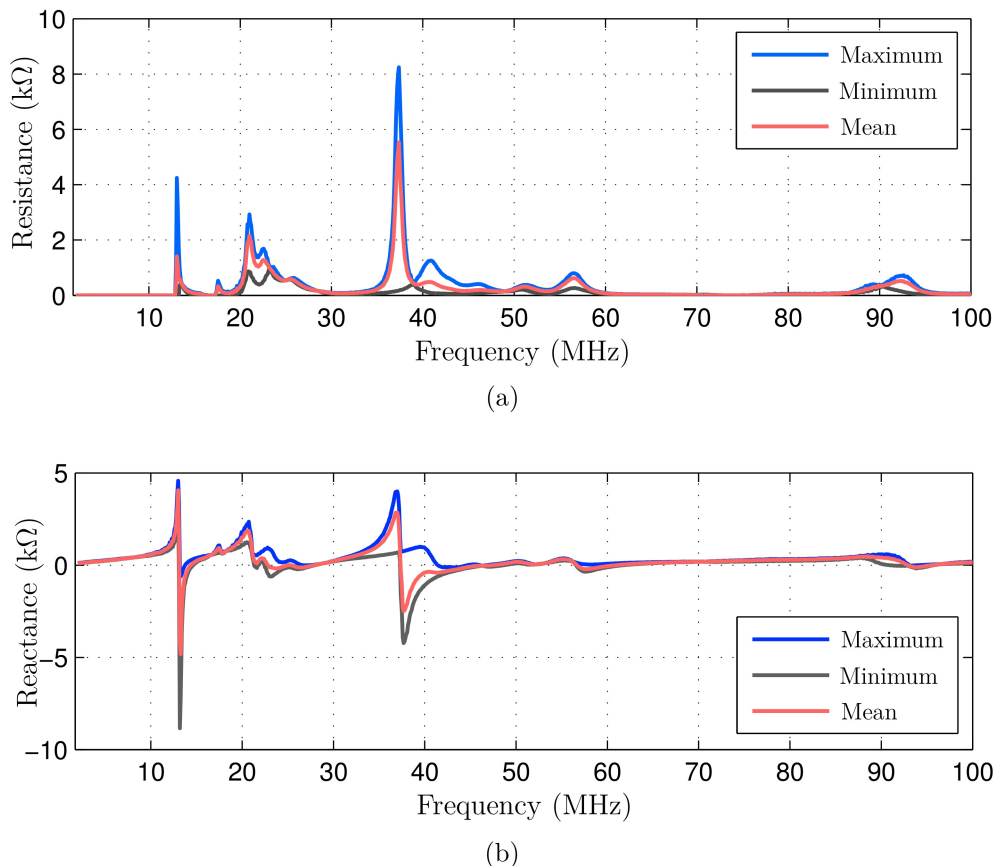
Figure 27: (a) Resistive and (b) Reactive components of the aircraft access impedance for CF #1.

Figures 28a and 28b show resistive and reactive components of the aircraft access impedance obtained from CF #2. In Figure 28a, the maximum resistance reaches 3.2 kΩ at frequency 39 MHz. On the other hand, in Figure 28b, the maximum reactive reaches 2.6 kΩ at frequency 57 MHz, whereas the minimum reaches −2.2 kΩ at same frequency.

Empirical cumulative distribution function (cdf) of resistive and reactive components of the aircraft access impedance for FB1 are illustrated in Figures 29 and 30, respectively. In Figure 29, for a probability less than or equal to 0.9, the measured values of resistance can reach 265 Ω and 568 Ω for CF #1 and CF #2, respectively.

The results depicted in Figure 30 for CF #1 show that the probability of the reactance to be capacity is less than or equal to 0.2, whereas for the CF #2 the probability is less than or equal to 0.002. Hence, for both measurement configuration, we practically have an inductive reactance. That is a common sense in electric power system field because the majority of loads are inductive. Also, we can note that for a probability
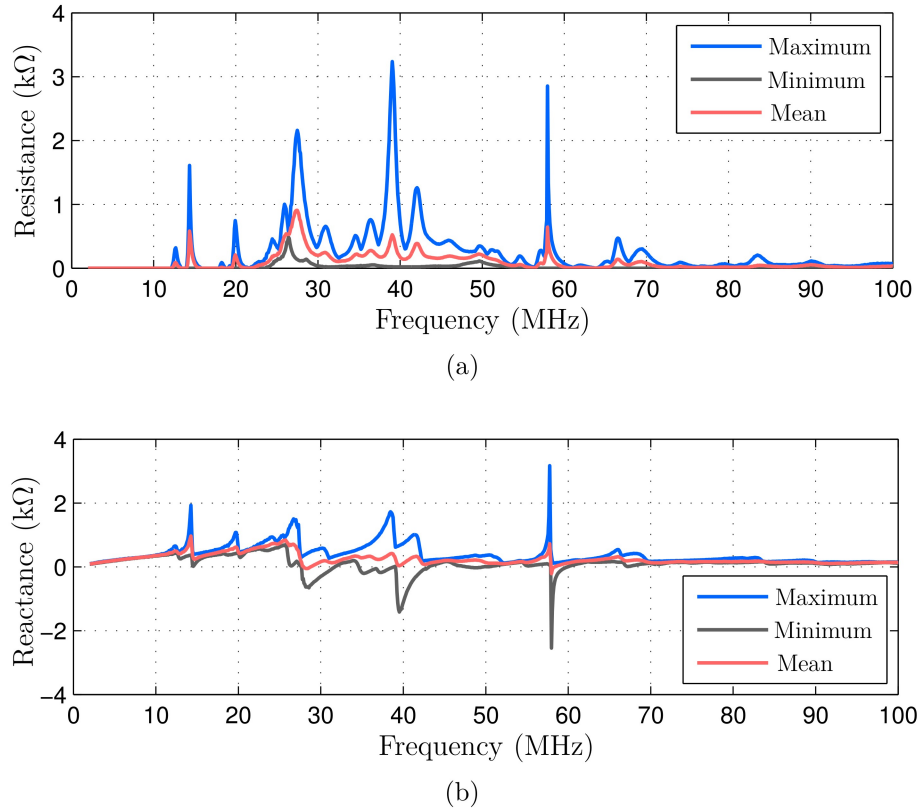
Figure 28: (a) Resistive and (b) Reactive components of the aircraft access impedance for CF #2.

interval between 0.9 and 0.1, the reactance does not varies significantly. Regarding this probability interval, it ranges between −159 and 710 Ω for CF #1 and between 70 and 534 Ω for CF #2.
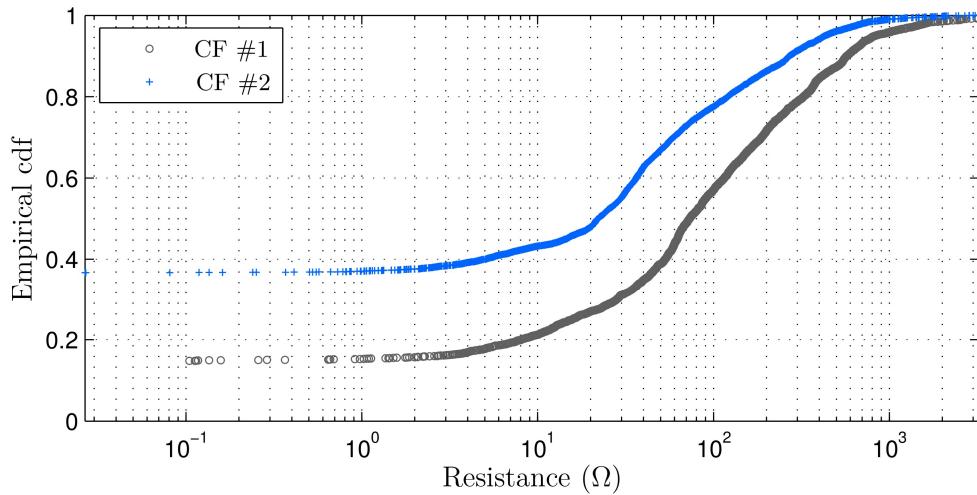
Figure 29: Empirical cdf of the real component of the measured access impedance in both measurement configurations.
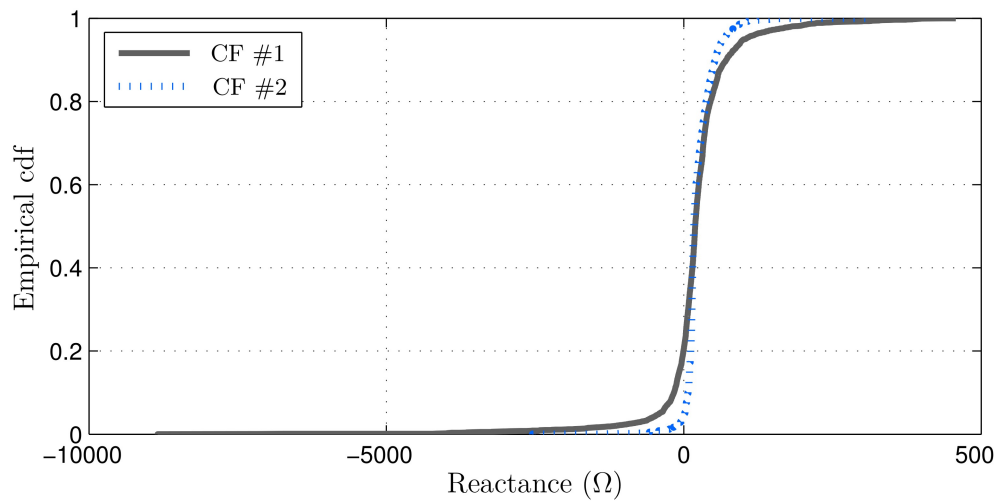
Figure 30: Empirical cdf of the imaginary component of the measured access impedance in both measurement configurations.

4.9 Summary

This chapter presented the characterization of the aircraft PLC channels for three distinct frequency bands: FB1, $1.7 - 30$ MHz; FB2, $1.7 - 50$ MHz; and FB3, $1.7 - 100$ MHz. This characterization was based on analyses of frequency response magnitude, ACA, coherence bandwidth, RMS-DS, coherence time, channel capacity, additive noise, and access impedance.

5 Conclusion

This work presented a detailed characterization of PLC channels over electric power grid of the flight test executive aircraft Legacy 450. The electric power grid investigated is responsible for delivering energy to the aircraft's instrumentation equipments of flight tests. With these regards, measurement campaign carried out in the aircraft Legacy 450 were outlined. The raw data was collected by considering two measurements configurations of power lines (CF #1 and CF #2). Statistical characterization of frequency response magnitude, ACG, coherence bandwidth, RMS-DS, coherence time, channel capacity, additive noise, and access impedance were assessed. The analysis was performed considering three frequency bands: $1.7 - 30$ MHz (FB1), $1.7 - 50$ MHz (FB2), and $1.7 - 100$ MHz (FB3). Analyses over the numerical results offered relevant information to design PLC technologies electric power grids in aircraft.

Based on the numerical analysis we showed the measurement configuration where the instrumentation equipments (loads) are physically connected (CF #2) is a better scenario for data communication than the one where the loads are connected to the electric power grid through different wire harnesses (CF #1). Furthermore, the results showed that the aircraft PLC channels have coherence time much higher than the Brazilian in-home ones. In fact, this difference can be six times in favor of aircraft PLC channels for CF #2. Also, the access impedance analysis pointed out that it is practically inductive, which is a common sense in electric power system field since the majority of loads are inductive.

Moreover, the statistical analysis of the aircraft PLC noise showed that it can be modeled by a Logistic probability distribution for both CF #1 and CF #2 in FB1 and for CF #1 in FB2. On the other hand, the noise can be modeled by a t Location-Scale probability distribution for CF #2 in FB2 and for both CF #1 and CF #2 in FB3.

The upper and the lower channel capacities computed, for FB3 and PSD$= -50$ dBm/Hz, are around 988 and 892 Mbps, respectively. However, due to the bound limit of CM current flowing on wires imposed by the aeronautic standard RTCA/DO-160G, the channel capacity for FB3 reaches only 100 Mbps. This result corroborates with previous works that pointed out to the use of DM to implement PLC technology aboard aircraft instead of CM if the CSD is not increased in the future.

Finally, but not the least, the comparison between aircraft and in-home PLC channels revealed that in-home PLC technology can be applied to aircraft PLC system without significative performance reduction.

5.1   Future Works

A list of future works are as follows:

- To carry out measurement campaign in others flight test aircrafts in order to obtain more information about characterize the aircraft electric power grids.

- To propose a model for the channel impulse response and/or channel frequency response of flight test aircraft PLC channels to assist the development of novel PLC technologies for aircraft.

- To specify, design, and prototype PLC modem suitable for flight test aircrafts.

REFERENCES

[1] Embraer, 2016. [Online]. Available: http://pt.embraerexecutivejets.com/en-us/jets/legacy-450/pages/overview.aspx.

[2] S. Barmada, L. Bellanti, M. Raugi, and M. Tucci, "Analysis of powerline communication channels in ships," *IEEE Transactions on Vehicular Technology*, vol. 59, no. 7, pp. 3161–3170, Sept. 2010.

[3] S. Barmada, A. Gaggeli, A. Musolino, R. Rizzo, M. Raugi, and M. Tucci, "Design of PLC system onboard trains: selection and analysis of the PLC channel," in *Proc. IEEE International Symposium on Power Line Communications and Its Applications*, Apr. 2008, pp. 13–17.

[4] M. Lienard, M. Carrion, V. Degardin, and P. Degauque, "Analysis of powerline communication channels in ships," *IEEE Transactions on Vehicular Technology*, vol. 57, no. 2, pp. 670–679, Mar. 2008.

[5] F. Grassi, S. A. Pignari, and J. Wolf, "Channel characterization and EMC assessment of a PLC system of spacecraft DC differential power buses," *IEEE Transactions on Electromagnetic Compatibility*, vol. 53, no. 3, pp. 664–675, Aug. 2011.

[6] C. H. Jones, "Communications over aircraft power lines," in *Proc. IEEE International Symposium on Power Line Communications and Its Applications*, Mar. 2006, pp. 149–154.

[7] O. Elgezabal and A. Sanz, "Modeling & simulating power line communications on civil aircraft: first steps," in *Proc. IEEE/AIAA Digital Avionics Systems Conference*, Oct. 2010, pp. 5B5, 1–16.

[8] V. Degardin, I. Junqua, M. Lienard, P. Degauque, and S. Bertuol, "Theoretical approach to the feasibility of power-line communication in aircrafts," *IEEE Transactions on Vehicular Technology*, vol. 62, no. 3, pp. 1362–1366, Mar. 2013.

[9] S. Dominiak, S. Serbu, S. Schneele, F. Nuscheler, and T. Mayer, "The application of commercial power line communications technology for avionics systems," in *Proc. IEEE/AIAA Digital Avionics Systems Conference*, Oct. 2012, pp. 7E1, 1–14.

[10] M. Tlich, A. Zeddam, F. Moulin, and F. Gauthier, "Indoor power-line communications channel characterization up to 100 mhz - part ii: Time frequency analysis," *IEEE Transactions on Power Delivery*, vol. 23, no. 3, pp. 1402–1409, Jul. 2008.

[11] J. A. Cortés, F. J. Canete, L. Díez, and J. L. G. Moreno, "On the statistical properties of indoor power line channels: Measurements and models," in *Proc. IEEE International Symposium on Power Line Communications and Its Applications*, Apr. 2011, pp. 271–276.

[12] A. M. Tonello, F. Versolatto, and A. Pittolo, "In-home power line communication channel: Statistical characterization," *IEEE Transactions on Communications*, vol. 62, no. 6, pp. 2096–2106, Jun. 2014.

[13] T. R. Oliveira, "The characterization of hybrid PLC-wireless and PLC channels in the frequency band between 1.7 and 100 mhz for data communication," Ph.D. dissertation, Federal University of Juiz de Fora, 2015.

[14] G. R. Colen, C. A. G. Marques, T. R. Oliveira, F. P. V. de Campos, and M. V. Ribeiro, "Measurement setup for characterizing low-voltage and outdoor electric distribution grids for plc systems," in *Proc. Conference on Innovative Smart Grid Technologies Latin America*, Apr. 2013, pp. 1–5.

[15] A. A. M. Picorone, R. Sampaio-Neto, and M. V. Ribeiro, "Coherence time and sparsity of brazilian outdoor plc channels: a preliminary analysis," in *Proc. IEEE International Symposium on Power Line Communications and Its Applications*, Mar. 2014, pp. 1–5.

[16] V. Degardin, P. Laly, M. Lienard, and P. Degauque, "Investigation on power line communication in aircrafts," *IET Communications*, vol. 8, no. 10, pp. 1868–1874, Jul. 2014.

[17] S. Bertuol, I. Junqua, V. Degardin, P. Deguaque, M. Dunand, and J. Genoulaz, "Numerical assessment of propagation channel characteristics for future applications of power line communication in aircraft," in *Proc. International Symposium on Electromagnetic Compability - EMC Europe*, Sept. 2011, pp. 506–511.

[18] S. Dominiak, H. Widmer, and M. Bittner, "A bifilar approach to power and data transmission over common wires in aircraft," in *Proc. IEEE/AIAA Digital Avionics Systems Conference*, Oct. 2011, pp. 7B4, 1–13.

[19] V. Degardin, P. Laly, M. Lienard, and P. Degauque, "A synthesis of theoretical and experimental study on power line communication over an aircraft tree-shaped network," in *Proc. URSI General Assembly and Scientific Symposium*, Aug. 2014, pp. 1–4.

[20] *RTCA/DO-160G - Environment conditions and test procedures for airborne equipment*, Radio Technical Commission for Aeronautics (RTCA) Std., Dec. 2010.

[21] E. L. Godo, "Flight control system with remote electronics," in *Proc. IEEE/AIAA Digital Avionics Systems Conference*, vol. 2, Oct. 2002, pp. 13B1, 1–7.

[22] M. D'Amore, K. Gigliotti, M. Ricci, and M. S. Sarto, "Feasibility of broadband power line communication aboard an aircraft," in *Proc. International Symposium on Electromagnetic Compability - EMC Europe*, Sept. 2008, pp. 1–6.

[23] J. O'Brien and A. Kulshreshtha, "Distributed and remote control of flight control actuation using power line communications," in *Proc. IEEE/AIAA Digital Avionics Systems Conference*, Oct. 2008, pp. 1D4, 1–12.

[24] I. Junqua, V. Degardin, M. Lienard, S. Bertuol, and P. Deguaque, "PLC in aircraft: channel modeling," in *Third Workshop on Power Line Communications*, Oct. 2009, pp. 1–3.

[25] V. Degardin, E. P. Simon, M. Morelle, M. Lienard, and P. Degauque, "On the possibility of using PLC in aircraft," in *Proc. IEEE International Symposium on Power Line Communications and Its Applications*, Mar. 2010, pp. 337–340.

[26] V. Degardin, M. Lienard, P. Degauque, and I. Junqua, "Power line communication in aircraft: Channel modelling and performance analysis," in *Proc. International Caribbean Conference on Devices, Circuits and Systems*, Mar. 2012, pp. 1–3.

[27] *ARINC-429*, Aeronautical Radio Inc Std., 2016. [Online]. Available: https://www.aim-online.com.

[28] *MIL-STD-1553*, United States Department of Defense Std., 2016. [Online]. Available: http://www.milstd1553.com.

[29] K. Kilani, V. Degardin, P. Laly, and M. Lienard, "Transmission on aircraft power line between an inverter and a motor: impulsive noise characterization," in *Proc. IEEE International Symposium on Power Line Communications and Its Applications*, Apr. 2011, pp. 301–304.

[30] S. Dominiak, G. Vos, T. ter Meer, and H. Widmer, "Achieving EMC emissions compliance for an aeronautics power line communications system," in *Proc. ESA Workshop on Aerospace EMC*, May 2012, pp. 1–6.

[31] V. Degardin, I. Junqua, M. Lienard, P. Degauque, S. Bertuol, J. Genoulez, and M. Dunand, "Predicted performances of power line communication in aircraft," in *Proc. ESA Workshop on Aerospace EMC*, May 2012, pp. 1–4.

[32] K. Kilani, V. Degardin, P. Laly, M. Lienard, and Degauque, "Impulsive noise generated by a pulse width modulation inverter: Modeling and impact on powerline communication," in *Proc. IEEE International Symposium on Power Line Communications and Its Applications*, Mar. 2013, pp. 75–79.

[33] *Homeplug AV specifications*, Homeplug Alliance Std. [Online]. Available: http://www.homeplug.org.

[34] C. Zhang, Y. Zhang, and L. Zhao, "Aircraft power line communications with non-continuous interferometry OFDM," in *Proc. IEEE/AIAA Digital Avionics Systems Conference*, Oct. 2013, pp. 3A1, 1–10.

[35] P. Degauque, I. S. Stievano, S. A. Pignari, V. Degardin, F. G. Canavero, F. Grassi, and F. J. Cañete, "Power-line communication: Channel characterization and modeling for transportation systems," *IEEE Vehicular Technology Magazine*, vol. 10, no. 2, pp. 28–37, Apr. 2015.

[36] T. Larhzaoui, F. Nouvel, J. Y. Baudais, V. Degardin, and P. Laly, "Analysis of PLC channels in aircraft environment and optimization of som OFDM parameters," in *Proc. International Conference on Systems and Networks Communications*, Oct. 2013, pp. 1–5.

[37] V. Degardin, K. Kilani, L. Kone, M. Lienard, and P. Degauque, "Feasibility of a high-bit-rate power-line communication between an inverter and a motor," *IEEE Transactions on Industrial Electronics*, vol. 61, no. 9, pp. 4816–4823, Dec. 2013.

[38] *Homeplug Green Phy specifications*, Homeplug Alliance Std. [Online]. Available: http://groups.homeplug.org.

[39] T. Larhzaoui, F. Nouvel, J. Y. Baudais, P. Degauque, and V. Degardin, "OFDM PLC transmission for aircraft flight control system," in *Proc. IEEE International Symposium on Power Line Communications and Its Applications*, Mar. 2014, pp. 220–225.

[40] J. Wassner, S. Dominiak, and J. M. Paya, "Model based design of an avionics power line communications physical layer," in *Proc. IEEE/AIAA Digital Avionics Systems Conference*, Sept. 2015, pp. 2C4, 1–11.

[41] Mathworks, 2016. [Online]. Available: http://www.mathworks.com/products/matlab.

[42] Xilinx, 2016. [Online]. Available: http://www.xilinx.com.

[43] T. R. Oliveira, C. A. G. Marques, W. A. Finamore, S. L. Netto, and M. V. Ribeiro, "A methodology for estimating frequency responses of electric power grids," *Journal of Control, Automation and Electrical Systems*, vol. 25, no. 6, pp. 720–731, Dec. 2014.

[44] Quartzlock, 2016. [Online]. Available: http://www.quartzlock.com.

[45] ACME, 2016. [Online]. Available: http://www.acmeportable.com.

[46] Gage, 2016. [Online]. Available: http://www.gage-applied.com.

[47] Agilent, 2016. [Online]. Available: http://www.home.agilent.com.

[48] L. G. S. Costa, "Circuitos de acoplamento para transceptores PLC (power line communications)," Master's thesis, Federal University of Juiz de Fora, 2012.

[49] M. V. Ribeiro, G. R. Colen, F. P. V. de Campos, and H. V. Poor, "Clustered-orthogonal frequency division multiplexing for power line communication: when is it beneficial," *IET Communications*, vol. 8, no. 13, pp. 2336–2347, Sept. 2014.

[50] J. D. V. Payán, "In-home and low-voltage channel characterization of non-cooperative and cooperative power line communication," Master's thesis, Federal University of Juiz de Fora, 2014.

[51] P. D. Welch, "The use of fast fourier transform for the estimation of power spectra: A method based on time averaging over short, modified perodograms," *IEEE Transactions on Audio and Electroacoustic*, vol. AU-15, no. 2, pp. 70–73, June 1967.

[52] T. M. Cover and J. A. Thomas, *Elements of information Theory.* John Wiley & Sons, 2006.

[53] A. M. Mood, F. A. Graybill, and D. C. Boes, *Introduction to the Theory of Statistics.* McGraw Hill, 1074.

[54] C. R. B. Cabral, V. H. Lachos, and C. B. Zeller, "Multivariate measurement error models mixtures of skew-student distributions," *Journal of Multivariate Analysis*, vol. 124, no. 0, pp. 179–198, Feb. 2014.

[55] T. R. Oliveira, C. B. Zeller, S. L. Netto, and M. V. Ribeiro, "Statistical modeling of the average channel gain and delay spread in in-home PLC channels," in *Proc. IEEE International Symposium on Power Line Communications and Its Applications*, Mar. 2015, pp. 184–188.

[56] G. R. Colen, "Resource allocation and time-frequency modulation for power line communication," Ph.D. dissertation, Federal University of Juiz de Fora, 2016.

[57] ANATEL, 2016. [Online]. Available: http://www.anatel.gov.br/legislacao/resolucoes/2009/101-resolucao-527.

[58] J. A. Canete, F. J.; Cortés, L. Díez, and J. T. Entrambasaguas, "A channel model proposal for indoor power line communications," *IEEE Communications Magazine*, vol. 49, no. 12, pp. 166–174, Dec. 2011.

[59] M. Zimmermann and K. Dostert, "Analysis and modeling of impulsive noise in broadband powerline communications," *IEEE Transactions on electromagnetic Compatibility*, vol. 44, no. 1, pp. 250–258, Feb. 2002.

[60] V. Fernades, S. Angelova, W. A. Finamore, and M. V. Ribeiro, "Analysis and modeling of impulsive noise in broad-band powerline communications," in *Proc. Brazilian Symposium of Telecommunications*, Set. 2015, pp. 1–5.

[61] D. Middleton, "Canonical non-gaussian noise models: Their implications for measurement and for prediction of receiver performance," *IEEE Transactions on electromagnetic Compatibility*, vol. 21, no. 3, pp. 209–220, Feb. 1079.

Appendix A – Parameters of Distributions

This appendix summarizes the parameters of the two best statistical distribution models offering the best fit to aircraft PLC noise data set collected from CF #1 and CF #2 for the FB1, FB2, and FB3 frequency bands.

Table 9: Parameters of the two best statistical distributions models for aircraft PLC noises from both measurement configurations.

FB1				
	Distribution	Parameter	Estimate	Standard Error
CF #1	Logistic	μ	0.001	0.000
		σ	0.001	0.000
	t Location-Scale	μ	0.001	0.000
		σ	0.001	0.001
		ν	8.362	0.100
CF #2	Logistic	μ	0.001	0.000
		σ	0.001	0.000
	t Location-Scale	μ	0.001	0.000
		σ	0.001	0.001
		ν	6.649	0.082
FB2				
	Distribution	Parameter	Estimate	Standard Error
CF #1	Logistic	μ	0.001	0.000
		σ	0.001	0.000
	t Location-Scale	μ	0.001	0.001
		σ	0.002	0.001
		ν	7.974	0.083
CF #2	Logistic	μ	0.001	0.000
		σ	0.001	0.000
	t Location-Scale	μ	0.001	0.001
		σ	0.002	0.001
		ν	11.162	0.113
FB3				
	Distribution	Parameter	Estimate	Standard Error
CF #1	Logistic	μ	0.001	0.000
		σ	0.002	0.000
	t Location-Scale	μ	0.001	0.000
		σ	0.003	0.001
		ν	8.664	0.075
CF #2	Logistic	μ	0.001	0.000
		σ	0.002	0.000
	t Location-Scale	μ	0.001	0.001
		σ	0.003	0.001
		ν	11.250	0.095

Appendix B – Statistical Distributions

This appendix summarizes the statistical distribution models considered in this work to model the aircraft PLC noise data sets.

- Bernoulli-Gaussian: According to [61], the pdf of an Bernoulli-Gaussian distribution can be expressed as a zero-mean Gaussian mixture weighted according to a Poisson distribution, so that it can be expressed as

$$f(x|\sigma^2, A, \Gamma) = \sum_{m=0}^{2} \frac{e^{-A} A^m}{m!} \frac{1}{\sqrt{2\pi\sigma_m^2}} e^{-\frac{x^2}{2\sigma_m^2}}, \qquad -\infty < x < \infty, \qquad (\text{B.1})$$

where the variance σ_m^2 is given by

$$\sigma_m^2 = \sigma_I^2 \frac{m}{A} + \sigma_G^2 = \sigma^2 \frac{\dfrac{m}{a} + \Gamma}{1 + \Gamma},$$

such as σ_I^2 and σ_G^2 are the impulsive and background Gaussian variances, respectively.

Parameters description:

- σ^2: variance.

- A: impulsive index.

- Γ: σ_G^2/σ_I^2.

In [60], the parameters optimized are $p = 1 - A$, $\alpha = \sqrt{1 + 1/(A\Gamma)}$, and σ^2.

- Logistic: The pdf of a Logistic distribution is given by

$$f(x|\mu, \sigma) = \frac{e^{-\frac{x-\mu}{\sigma}}}{\sigma \left(1 + e^{-\frac{x-\mu}{\sigma}}\right)^2}, \qquad -\infty < x < \infty. \qquad (\text{B.2})$$

Parameters description:

- μ: location.

- σ: scale.

- Normal: The pdf of a Normal distribution can be expressed as

$$f(x|\mu, \sigma) = \frac{1}{\sqrt{2\pi\sigma_m^2}} e^{-\frac{(x-\mu)^2}{2\sigma_m^2}}, \qquad -\infty < x < \infty. \qquad (\text{B.3})$$

Parameters description:

- μ: mean.

- σ: standard deviation.

- t Location-Scale: The pdf of a t Location-Scale distribution is described by

$$f(x|\mu,\sigma,\nu) = \frac{\Gamma\left(\frac{\nu+1}{2}\right)}{\sigma\sqrt{\nu\pi}\,\Gamma\left(\frac{\nu}{2}\right)} \left[\frac{\nu\left(\frac{x-\mu}{\sigma}\right)^2}{\nu}\right]^{-\frac{\nu+1}{2}}, \qquad -\infty < x < \infty, \qquad \text{(B.4)}$$

where $\Gamma(\cdot)$ is the Gamma function.

Parameters description:

- μ: location.

- σ: scale.

- ν: shape.

Appendix C – Publications

The list of journal papers written or submitted during the graduate period is as follows:

- Â. Camponogara, T. R. Oliveira, R. Machado, W. A. Finamore, and M. V. Ribeiro, "Characterization of Aircraft PLC Channels: Frequency Response, Additive Noise, and Access Impedance," *IEEE Transactions on Communication*, 2016, under review process.

- M. L. G. Salmento, E. P. de Aguiar, Â. Camponogara, and M. V. Ribeiro, "Reduced Rank Adaptive Filter, Set-Membership, and Variable Step Size for Impulsive UWB-based PLC Systems," *Digital Signal Processing*, 2016, under review process.

- M. L. G. Salmento, Â. Camponogara, and M. V. Ribeiro, "A Novel Synchronization Scheme for Impulsive UWB-based PLC Systems," *IEEE Transactions on Latin America*, 2016, under review process.

The list of conference papers published during the graduate period is as follows:

- Â. Camponogara, R. Machado, and M. V. Ribeiro, "Improving the Performance of MIMO PLC System with Feedback Information: Time-Varying Channel Analysis," in *Proc. Brazilian Symposium of Telecommunications*, pp. 1-5, Sept. 2015.

- Â. Camponogara, T. R. Oliveira, R. Machado, W. A. Finamore, F. P. V. de Campos, and M. V. Ribeiro, "Aircraft PLC Channels Characterization: Initial Discussion," in *Proc. Brazilian Symposium of Telecommunications*, pp. 1-5, Aug. 2016.